(2)

AD_____

CONTRACT NO: DAMD17-89-C-9133

TITLE: SEALED ROTATING ANODE X-RAY TUBE WITH ENHANCED POWER AND DUTY CYCLE

PRINCIPAL INVESTIGATOR: J.W. Motz

CONTRACTING ORGANIZATION: Rayex Corporation
9701 Fields Road #1605
Gaithersburg, MD 20878

REPORT DATE: February 20, 1990

TYPE OF REPORT: Phase I Final Report

PREPARED FOR: U.S. ARMY MEDICAL RESEARCH AND DEVELOPMENT COMMAND
Fort Detrick, Frederick, Maryland 21702-5012

DISTRIBUTION STATEMENT: Approved for public release;
distribution unlimited

The findings in this report are not to be construed as an official Department of the Army position unless so designated by other authorized documents.

REPORT DOCUMENTATION PAGE

Form Approved
OMB No. [illegible]

AGENCY USE ONLY (Leave blank)	REPORT DATE	REPORT TYPE AND DATES COVERED
	20 February 1990	Final Phase I (8/15/89 - 2/15/90)

TITLE AND SUBTITLE
Sealed Rotating Anode X-Ray Tube with Enhanced Power and Duty Cycle

FUNDING NUMBERS
Contract No.
DAMD17-89-C-9133

AUTHOR(S)
Dr. J. W. Motz

PERFORMING ORGANIZATION NAME(S) AND ADDRESS(ES)
Rayex Corporation
9701 Fields Road, #1605
Gaithersburg, MD 20878

PERFORMING ORGANIZATION REPORT NUMBER

SPONSORING/MONITORING AGENCY NAME(S) AND ADDRESS(ES)
U.S. Army Medical Research & Development Command
Fort Detrick
Frederick, Maryland 21702-5012

Approved for public release; distribution unlimited

A new design of a sealed rotating anode X-ray tube has been developed which has an X-ray emission power that is a factor of 1.4, 1.6, and 2.0 greater than present-day X-ray tubes operating respectively at 50, 150, and 300 kilovolts with the same target heat load. These power factors are predicted by extensive Monte Carlo calculations relating to electron diffusion and X-ray production in a tungsten target. The tube design incorporates a state-of-the-art metal-ceramic structure which is air cooled and which has many important advantages over present-day rotating anode tubes.

Enhanced X-ray power, rotating anode tube, metal ceramic tube, electron gun design, tomography, radiological equipment

Unclassified | Unclassified | Unclassified | Unlimited

APPENDIX B
DOD No. 89.1

U.S. DEPARTMENT OF DEFENSE

SMALL BUSINESS INNOVATION RESEARCH (SBIR) PROGRAM
PHASE I - FY 1989
PROJECT SUMMARY

Topic No. 084 Military Department/Agency ARMY.

Name and Address of Proposing Small Business Firm

Rayex Corporation
9701 Fields Rd #1605
Gaithersburg, MD 20878

Name and Title of Principal Investigator

Dr. J. W. Motz

Proposal Title

Sealed Rotating Anode X-Ray Tube with Enhanced Power and Duty Cycle

Technical Abstract (Limit your abstract to 200 words with no classified or proprietary information/data.)

A new design of a sealed rotating anode X-ray tube has been developed which has an X-ray emission power that is a factor of 1.4, 1.6, and 2.0 greater than present-day X-ray tubes operating respectively at 50, 150, and 300 Kilovolts with the same target heat load. These power factors are predicted by extensive Monte Carlo calculations relating to electron diffusion and X-ray production in a tungsten target. The tube design incorporates a state-of-the-art metal-ceramic structure which is air cooled and which has many important advantages over present-day rotating anode tubes.

Anticipated Benefits/Potential Commercial Applications of the Research or Development

The benefits expected from this enhanced power rotating anode X-ray tube are:

* Increased patient throughput for CAT examinations
* Longer tube life
* Reduced maintenance costs, less down time
* Better image quality with improved focal spot characteristics and reduced off-focus radiation

List a maximum of 8 Key Words that describe the Project.

Enhanced X-ray power, rotating anode tube, metal ceramic tube, electron gun design, tomography, radiological equipment

I. INTRODUCTION

The maximum X-ray power output from an X-ray tube is an important parameter in the operation and maintenance of a radiological system. The time period required to inspect an object is inversely proportional to the X-ray power output. In addition, for a given X-ray power output of the X-ray tube, the tube lifetime is directly proportional to its maximum power rating. Accordingly, the effect of using X-ray tubes with higher values for the maximum X-ray power output than presently available, is to reduce the inspection times and the throughput of patients or objects examined with the radiological system, as well as to reduce the maintenance and operating costs because of the longer tube lifetimes.

The purpose of this Phase I program is to show the feasibility of enhancing the X-ray power output and duty cycle of rotating anode X-ray tubes by modifying the Standard Tube geometry according to the method described below. The power enhancement factors obtained in this study are equally applicable to stationary as well as rotating anode X-ray tubes.

The method proposed in this study to enhance tube X-ray power output may be explained by referring to Figure 1 *(page 20)*, where α is the incident angle *(also designated as the obliquity angle)* of the electron beam with respect to the plane of the target surface. Various electron backscattering calculations have shown that for a given incident electron energy, the fraction of the electron beam energy deposited in the anode decreases as this incident angle decreases. In addition, an analysis of the results obtained in a previous study given in reference [1] *(page 34)* shows that the total x-ray energy output from the anode is not linearly proportional to the electron energy deposited in the target for different incident angles of the electron beam. The implication of this result is that for a given tube kilovoltage, there is an optimum tube geometry involving the incident electron beam angle and the x-ray emission angle, which provides the maximum value for the x-ray output energy per unit electron beam energy deposited in the anode. The significant parameter that limits tube power is the electron beam energy deposited in the target rather then the incident beam energy. Accordingly, the method used in this study to enhance tube power is first to determine the optimum tube geometry, and then to determine the X-ray power enhancement factor given by the ratio of the x-ray output energy per unit electron energy deposited in the target respectively for the optimum geometry and for the standard geometry used in present day tubes.

The primary goals in this Phase I study are as follows:

(1) design a rotating anode X-ray tube which operates at 150 Kilovolts and which has the optimum geometry for producing the maximum X-ray power output.

(2) determine the X-ray power enhancement factors over the region from 50 to 500 Kilovolts, that can be obtained with tubes having the optimum geometry compared with present-day tubes having the standard geometry.

The steps that were taken to achieve these goals are discussed in the following sections.

II. PHASE I TECHNICAL OBJECTIVES

There are certain technical objectives which must be achieved in this Phase I program in order to demonstrate the technical feasibility of developing a Sealed, Rotating Anode X-Ray Tube with Enhanced Power and Duty Cycles. These objectives may be specified as follows:

* Carry out detailed theoretical calculations on X-ray production by electrons with initial energies in the region from 50 to 500 keV. These calculations will provide detailed data on the differential dependence of (a) the X-ray spectra, (b) the angular distribution of the scattered electron energy, and (c) the fraction of the incident electron beam energy deposited in the target, on the various parameters involved in the tube design including the incident electron energy, the incident electron angle, and the X-ray emission angle.

* Determine the optimum tube geometry for producing the maximum X-ray power output from the theoretical data.

* Determine the X-ray power enhancement factors from the theoretical data for tubes with the optimum geometry operating over the region from 50 to 500 kilovolts.

* Design a 150 Kilovolt rotating anode X-ray tube with the optimum geometry for obtaining the enhanced X-ray power output.

III. THEORETICAL PREDICTIONS OF X-RAY PRODUCTION

The data required to determine the optimum tube geometry for maximum X-ray power output were obtained from detailed Monte Carlo calculations of the electron energy albedo in a tungsten target. These calculations included a detailed account of the electron scattering, penetration, and energy losses in the target for specified incident electron energies, as well as a quantitative description of the energy and angular distributions of the accompanying X-

rays. These calculations were carried out by Dr. Martin J. Berger who is one of the leading pioneers and experts on theoretical studies of the penetration, diffusion, and slowing down of high-energy radiations in bulk matter, and on the application of the Monte Carlo method to the calculation of the transport of gamma rays, bremsstrahlung, and electrons. The high accuracy and reliability of these statistical calculations has been confirmed and established from experience over a period of thirty years.

A. Nomenclature

Because of the large number of parameters, figures, and tables involved in this study, it is important to carefully define the symbols associated with the various parameters. Definitions of these symbols are given in the following list which may be used as a reference in this report.

T = incident electron kinetic energy, T' = scattered electron kinetic energy

$\mathbf{p}$ = electron momentum vector

$\mathbf{z}$ = vector perpendicular to the plane of the target surface

k = photon energy; $\mathbf{k}$ = photon momentum vector

k_c = minimum cutoff photon energy = 10 keV *(in this study)*

e = electron charge = $\mathbf{1.60 \times 10^{-19}}$ Coulombs

E_T = incident electron beam energy

E_T' = total energy of electrons emitted from target

E_D = electron energy deposited in target for given E_T

= $E_T - E_T' - E_X$

E_X = total photon energy emitted from target for given E_T and k_c

α = incident electron beam angle between the plane of the target surface and the electron momentum vector, $\mathbf{p}$.

θ = photon emission angle between the plane of the target surface and the photon momentum vector, $\mathbf{k}$.

θ_e = electron emission angle between the plane of the target surface and the momentum vector, $\mathbf{p}'$, of the scattered electron.

φ = azimuthal angle between the incident plane (**p**, **z**) and the emission plane, (k, **z**).

N = number of X-ray photons

n = number of electrons

$N(k,\theta,\varphi)$ = photon number distribution emitted from target with dependence on k per unit energy interval (averaged over 5 keV intervals [or 2 kV intervals for T equal to 50 keV]), θ (averaged over 5 degree intervals), and φ (averaged over 10 degree intervals:
- per unit solid angle
- per incident electron
- for given T and α

$N(k,\theta)$ = photon number distribution emitted from target with dependence on k per unit energy interval *(averaged over 5 keV intervals [or 2 keV intervals for* T *equal 50 keV])* and θ *(averaged over 5 degree intervals)*:
- averaged over φ between -10 and +10 degrees
- per unit solid angle
- per incident electron
- for given T and α

$E_X(\theta,\varphi)$ = angular distribution of photon energy emitted from target with dependence on θ *(averaged over 5 degree intervals)* and φ *(averaged over 10 degree intervals)*:
- integrated over k from k_c to T
- per unit solid angle
- per incident electron
- for given T and α

$E_X(\theta)$ = angular distribution of photon energy emitted from target with dependence on θ *(averaged over 5 degree intervals)*:
- averaged over φ between -10 and +10 degrees
- integrated over k from k_c to T
- per unit solid angle
- per incident electron
- for given T and α

$n(T')$ = electron number distribution emitted from target with dependence on T' per unit energy interval *(averaged over 5 keV intervals)*:
- averaged over φ between -180 and +180 degrees
- averaged over θ_e between 0 and 180 degrees
- per unit solid angle
- per incident electron
- for given T and α

$n(\theta_e)$ = electron angular distribution emitted from target with dependence on θ_e per unit energy interval (averaged over 5 keV intervals):
- averaged over φ between -180 and +180 degrees
- integrated over T' between 0 and T
- per unit solid angle
- per incident electron
- for given T and α

B. Method of Calculations.

The geometry used for these calculations is shown in Figure 1. The electron beam is incident on a tungsten target such that α is the incident angle *(also designated as the obliquity angle)* of the electron momentum vector, p, with respect to the plane of the target surface. The incident plane is defined by the two vectors *(p, z)* where **z** is the normal vector to the target plane. The x-ray emission angle θ is defined as the angle between the photon momentum vector, **k**, and the plane of the target surface, and the emission plane is defined by the two vectors *(**k**, **z**)*. The calculations also include the third directional parameter, namely the azimuthal angle, φ, between the incident and emission planes as shown in Figure 1.

The production of x-rays in a tungsten target, and the penetration and diffusion of the x-rays and electrons in this target, are calculated by the Monte Carlo method, using the electron-photon transport code ETRAN. In regard to photon transport, this code uses a conventional Monte Carlo model in which all successive photon scatterings are sampled. In regard to electron transport ETRAN is based on a condensed-random walk model, reference [2], in which angular deflections and energy losses of electrons in successive short path segments are sampled from appropriate distributions given by multiple-scattering and straggling theories. An overview of the ETRAN code can be found in reference [3]. The reliability and capabilities of ETRAN are discussed in reference [4], and also in reference [5] where a series of transport programs are discussed which borrow the Monte Carlo model from ETRAN but treat

more complex source-target configurations. The x-ray production cross sections used in ETRAN are described in reference [6], and the photon scattering and absorption cross sections in reference [7]. In addition to the x-rays produced when electrons are slowed down in the field of atoms and atomic electrons, the calculations also take into account the characteristic x-rays produced when electrons are ejected from the K shell of tungsten. Characteristic x-rays from the L-shell are neglected.

Each electron Monte Carlo history is followed until the electron's energy falls below 10 keV. The histories of secondary x-rays and characteristic x-ray photons are also followed down to 10 keV. For each combination of initial electron energy and direction of incidence, a sample of 100,000 electron histories is followed, and samples of 10 million histories of x-rays and 10 million histories of characteristic x-rays. The results are adjusted by means of a weight factor *(much smaller than unity)* to take into account the natural rate of photon production.

C. Summary of Cases and Tables

Calculations were done for 56 cases including seven initial electron energies (T = 500, 400, 300, 200, 150, 100 and 50 keV) and eight incident electron beam angles (α = 90, 70, 50, 30, 20, 10, and 2 degrees). The basic output obtained with the ETRAN code for X-ray production gives the quantity, N (k, θ, φ), for a semi-infinite tungsten medium. The photon energy bins include three windows with a width of 0.1 keV for the tungsten K X-ray energies (67.3, 59.3, and 58.0 keV) in order to facilitate the separation of unscattered K X-rays from the continuous photon spectrum.

The calculations for the 56 cases generate approximately 10 Megabytes of information to be stored on 5.25" floppy disks which can be read and utilized with an IBM compatible computer operating under the MS-DOS or PC-DOS operating system. Several processing codes were written which use this basic database in order to generate output tables. For each initial electron energy, 51 tables of processed output are provided. These tables will be stored on 5.25" floppy disks, so that their contents are available for further computer calculations.

In the present study, only a small fraction of the above data is used to demonstrate the feasibility of enhancing the X-ray power output by modifying the tube geometry. (In the future we plan to issue a separate comprehensive report with most of the data obtained in the present study). The data are given in the form of output tables which evaluate various quantities of interest as defined in Section III A. Samples of these tables are given in Tables 1, 2, 3, and 4 *(pages 40 - 45)* as follows:

Table 1: Evaluation of N (k, θ) for T = 150 keV, α = 90 degrees, and φ averaged between -10 and +10 degrees.

Table 2: Evaluation of E_x (θ, φ) for T = 150 keV and α = 90 degrees.

Table 3: Evaluation of $E_{T'} / E_T$, E_x / E_T , E_D , and E_x / E_D for T = 150 keV and for α = 90, 70, 50, 30, 20, 10, 5 and 2 degrees.

Table 4: Evaluation of $E_x(\theta)$ and $E_x(\theta) / E_D$ for T = 100 keV and for α = 90, 70, 50, 30, 20, 10, 5, and 2 degrees.

IV. THEORETICAL RESULTS

The results of the Monte Carlo calculations that are pertinent to the goals of this program are given in the following Sections.

A. X-ray Emission Energies, E_x and $E_x(\theta)$

The ratio of the X-ray emission energy, E_x, to the incident electron beam energy, E_T, is given in Figure 2 as a function of the incident electron angle, α, for incident electron energies, T, of 50, 100, 150, 200, 300, 400, and 500 keV. The X-ray energy, E_x, is integrated over the X-ray energies from the minimum cutoff energy, kc, of 10 keV to the maximum energy, T, and over the X-ray emission angles, θ and φ, from 0 to 180 degrees. These calculations were made for one incident electron such that $E_T = T$.

The dependence of the X-ray emission energy, $E_x(\theta)$, on the emission angle, θ, is given in Figure 3 for incident electron angles, α, of 10 and 70 degrees and for incident electron energies of 50, 150, and 500 keV. In this case, $E_x(\theta)$, is integrated over the X-ray energies from k_c (10 keV) to T, and is averaged over φ from -10 to +10 degrees.

Also, for a given emission angle, θ, in the interval from 5 to 10 degrees, the dependence of $E_x(\theta)$, on the incident electron angle, α, is given in Figure 4 for incident electron energies of 50, 150, and 500 keV. As defined in Section III A, these energies are expressed in keV units per unit solid angle per incident electron.

B. Electron Deposition Energy, E_D

The electron deposition energy, E_D, is expressed in terms of the fraction, E_D / E_T, where E_T is the incident electron beam energy. Figure 5 shows the dependence of E_D / E_T, on the incident electron angle, α, for incident electron energies of 100 and 500 keV. The data obtained for the electron energies of 50, 150, 200, 300, and 400 keV show that for a given value of the incident electron angle, α, the energy deposition fraction is approximately independent of the incident electron energy within the region from 50 to 500 keV. The results in Figure 5 show that the energy deposition fraction, E_D / E_T, increases from approximately 0.25 for $\alpha = 5$ degrees to 0.62 for $\alpha = 90$ degrees for incident electron energies in the region from 50 to 500 keV.

C. Energy Ratio of X-ray Emission to Electron Deposition

The energy ratio of X-ray emission to electron deposition, E_x / E_D, is given in Figure 6 as a function of the incident electron angle, α, for incident electron energies, T, of 50, 100, 150, 200, 300, 400, and 500 keV. These curves show a general behavior in which the total X-ray emission energy per unit electron energy deposited in the target decreases as the incident electron angle, α, increases from 0 to 90 degrees for incident electron energies in the region from 50 to 500 keV. This result is the first indication that there is an optimum tube geometry involving α for obtaining the maximum X-ray power output from the tube.

The key parameter for determining the optimum tube geometry to get the maximum X-ray power output is the energy ratio, $E_x(\theta) / E_D$, where $E_x(\theta)$ is the X-ray energy integrated from k_c to T for a given emission angle, θ, averaged over φ between -10 and +10 degrees, and E_D is the electron deposition energy in the target. The dependence of $E_x(\theta) / E_D$ on the incident electron angel, α, is shown in Figure 7 for an emission angle, θ, in the interval from 5-10 degrees, and for incident electron energies of 50, 100, 150, 200, 300, 400, and 500 keV. For each incident electron energy, the energy ratio, $E_x(\theta) / E_D$, decreases as α increases from 2 to 90 degrees. These are the basic curves that will be used to determine (a) the optimum tube geometry and (b) the power enhancement factors that can be obtained with the optimum geometry compared to the present day standard tube geometry.

V. The Optimum Tube Geometry

The tube geometry that relates to the X-ray power output in this study, involves the X-ray emission angle, θ, and the incident electron angle, α, as shown in Figure 1. The optimum tube geometry is defined as the **combination** of values for θ and α that provides the maximum X-ray emission energy for a given heat load on the target. This optimum geometry will be used in the design of the Enhanced Power tube. The procedure for determining this optimum geometry is described below.

A. The X-ray Emission Angle

The selection of the X-ray emission angle, θ, involves a tradeoff between the X-ray emission power and the area of the X-ray beam at a given distance from the target. As the value of θ approaches zero, the X-ray beam size at a given distance from the target is reduced because of the beam cutoff imposed by the target surface *(heel effect)*. At the same time, the actual area of the focal spot on the anode may be increased as the emission angle decreases, without changing the projected size of the focal spot area. For certain radiological procedures that require X-ray beams large enough to cover the chest area such as angiography, the value of θ is approximately 15 degrees. For X-ray beams with a small spread in θ, such as the fan beams used in CT machines, the value of θ is approximately 10 degrees. In the present study, the tube will be designed to produce fan beams for CT machines, and the value of θ for both the Standard and the Enhanced Power tube geometries is selected to be 10 degrees.

B. The Incident Electron Angle

The results in Figure 7 show that the maximum X-ray emission energy per unit electron deposition energy in the target is produced for an incident electron angle, α, of approximately 10 degrees. (This optimum value is not critical and may be specified within $\pm$ 2 degrees with less than a 10% change in the value of the energy ratio, $E_x(\theta) / E_D$. By comparison, the incident electron angle for the Standard geometry used in present day tubes is equal to approximately 80 degrees.

VI. The Enhanced Power Tube versus the Standard Tube

A summary of the differences between the Enhanced Power (EP) tube proposed for development in this Phase I study, and the typical Standard (S) tube used in present-day radiological systems, is given in the following sections. For a specified tube kilovoltage, these differences refer to the tube geometry and the tube performance with regard to the X-ray emission power, the target heat load, and the tube current.

A. Geometry

The tube geometry pertains to the electron incident angle, α, and the X-ray emission angle, θ, as shown in Figure 1. The EP tube is designed with the optimum geometry described in Section V, such that both α and θ are equal to approximately 10 degrees. Also as described in Section V, the S tube is designed with α equal to 80 degrees and θ equal to 10 degrees.

B. X-ray Power Enhancement Factor

The dependence of the energy ratio, $E_X(\theta) / E_D$, on the incident electrton angle, α, is given in Figure 7 for an X-ray emission angle, θ, averaged over the interval from 5 to 10 degrees, and for incident electron energies of 50, 100, 150, 200, 300, 400, and 500 keV. As defined in Section III A, $E_X(\theta)$, is the X-ray emission energy and E_D, is the electron deposition energy which is equivalent to the target heat load. The energy ratio for the EP tube, r_{EP}, is evaluated at α equal to 10 degrees, such that

$$r_{EP} = [\, E_X(\theta = 10^o) / E_D \,]_{\alpha = 10^o} \qquad (1)$$

The energy ratio for the S tube, r_S, is evaluated at α equal to 80 degrees, such that

$$r_S = [\, E_X(\theta = 10^o) / E_D \,]_{\alpha = 80^o} \qquad (2)$$

The **X-ray Power Enhancement Factor**, P, of the EP tube over the S tube for the same target heat load (or same value of E_D) is given by the equation

$$P = r_{EP} / r_S = [\, E_X(\theta = 10^o) \,]_{EP} / [\, E_X(\theta = 10^o) \,]_S \qquad (3)$$

From the curves in Figure 7, the X-ray **Power Enhancement Factor** was evaluated for the different electron energies *(or tube kilovoltages).*

The results in Figure 8 show that the X-ray **Power Enhancement Factor** increases with tube kilovoltage from approximately 1.4 at 50 kilovolts, to 2.4 at 500 kilovolts.

C. Target Heat Load

The target heat load is essentially equivalent to the electron deposition energy, E_D, and is an important factor in determining the lifetime of the X-ray tube. A comparison of the target heat loads for the EP and S tubes can be made by evaluating the heat load ratio, H, which is defined as

$$H = [\, E_D \,]_{EP} / [\, E_D \,]_S \qquad (4)$$

where the subscripts refer to the EP and S tubes. For the same X-ray emission energy, the heat load ratio, H, is equal to the reciprocal of the X-ray **Power Enhancement Factor**, P, such that from Equations (1), (2) and (3),

$$H = r_S / r_{EP} = 1 / P \qquad (5)$$

Accordingly, H may be evaluated at any given kilovoltage by taking the inverse value of P in Figure 8. For example at 150 kilovolts, H is equal to 1 / 1.6 or 0.63.

D. Tube Current

The currents required for the EP tube, I_{EP}, and the S tube, I_S, may be compared for the cases where (1) the target heat loads $[\, E_D \,]_{EP}$ and $[\, E_D \,]_S$, are equal, and (2) the X-ray emission energies $[\, E_X(\theta = 10^o) \,]_{EP}$ and $[\, E_X(\theta = 10^o) \,]_S$, are equal. To make this comparison, it is noted that the current ratio, I_{EP} / I_S, is equal to the corresponding ratio of incident electron beam energies, $[\, E_T \,]_{EP} / [\, E_T \,]_S$.

(1) Current Ratio for Same Target Heat Load

The target heat load fraction (or electron deposition energy fraction) is evaluated in Figure 5 as a function of the incident electron angle, α. The fractions for the EP and S tubes are given as

$$F_{EP} = [\, E_D / E_T \,]_{\alpha=10^o} = 0.31$$
$$F_S = [\, E_D / E_T \,]_{\alpha=80^o} = 0.62 \qquad (6)$$

For the same target heat load,

$$F_S / F_{EP} = [\, E_T \,]_{EP} / [\, E_T \,]_S = I_{EP} / I_S \qquad (7)$$

Then from Equations (6) and (7),

$$I_{EP} = 2I_S \qquad (8)$$

for any tube kilovoltage in the region from 50 to 500 kilovolts.

(2) Current Ratio for Same X-Ray Emission Energy

From Equation (6), we may write

$$(F_S / F_{EP}) = ([E_T]_{EP} / [E_T]_S) ([E_D]_S / [E_D]_{EP}) = 2 \qquad (9)$$

Then for the same X-ray Emission Energy, we have from Equations (1), (2), and (3):

$$r_s / r_{EP} = 1 / P = [E_D]_{EP} / [E_D]_S \qquad (10)$$

Accordingly from Equations (9) and (10), we have the equation

$$I_{EP} = 2\, I_S / P \qquad (11)$$

where P is evaluated in Figure 8 for a given kilovoltage. For example, at 150 kV, P is equal to 1.6, and I_{EP} is equal to approximately 1.3 I_S.

E. X-Ray Spectrum

The unfiltered X-ray spectrum obtained from the Monte Carlo data is given in Figures 9 and 10 respectively for the Standard (S) tube and the Enhanced Power (EP) tube, each operating at 150 kilovolts. The ordinate values in these Figures give the quantity, $N(k,\theta)$, which is defined in Section III A, with θ averaged over the interval from 5 to 10 degrees, and with α equal to 70 degrees and 10 degrees respectively for

the S and EP tubes. (For this comparison, the spectral shape at 70 degrees is not appreciably different from that at the designated angle of 80 degrees for the S tube). The results in Figures 9 and 10 show that there are no large differences in the spectral shapes except that the EP tube appears to have a harder (more photons) spectrum above 130 keV.

F. Comparison Chart

A summary of the differences between the EP and S tubes is given in Table 5 *(below)*. These differences pertain to the tube geometry, the X-ray emission power and the current requirements. This table may be used as a reference to estimate the X-ray power output and tube current requirement for the EP tube compared to a typical Standard Tube operating in present-day radiological Systems.

Table 5

Comparison of the Enhanced Power (EP) and the Standard (S) X-Ray Tubes.

		Standard Tube	Enhanced Power Tube
1.	Geometry		
	a. X-Ray emission angle, θ	10 degrees	10 degrees
	b. Incident electron angle, α	80 degrees	10 degrees
	c. Azimuthal angle, φ	0 degrees	0 degrees
2.	X-ray Power Enhancement Factor (EP Tube / S Tube), same target heat load		
	a. 50 kV	1.0	1.4
	b. 150 kV	1.0	1.6
	c. 300 kV	1.0	2.0
	d. 500 kV	1.0	2.4
3.	Target Heat Load Ratio (EP Tube / S Tube), same X-ray emission power		
	a. 50 kV	1.0	0.71
	b. 150 kV	1.0	0.63
	c. 300 kV	1.0	0.50
	d. 500 kV	1.0	0.42
4.	Tube Current Ratio (EP Tube / S Tube) Same target heat load, and same X-ray emission power		
	a. Same target heat load	1.0	2.0
	b. Same X-ray emission power		
	50 kV	1.0	1.42
	100 kV	1.0	1.26
	300 kV	1.0	1.00
	500 kV	1.0	.82

VII. Design of the Enhanced Power Tube

The design of the Enhanced Power tube with the specifications described in Section VI was subcontracted and carried out under the direction of Dr. Martin Braun. Dr. Braun has extensive experience as a tube designer at various tube manufacturing companies, and has been a pioneer in the development of an air-cooled rotating anode metal ceramic tube which will be incorporated in the design of this Enhanced Power tube. This tube will be designed for a maximum kilovoltage of 150 kilovolts so that the tube can operate in the range from 120 to 150 kilovolts, which is the usual operating range for tubes used in present CT systems.

A. Design of the Electron Gun

In the EP tube design, the incident electron beam angle, α, of 10 degrees is equal to the X-ray emission angle, θ, and the projected X-ray beam shape is approximately the same as the electron beam cross section. It should be noted that for most X-ray tubes, the X-ray emission angle, θ, is of the order of 7 to 13 degrees with a typical value of 10 degrees.

In order to retain compatibility with existing X-ray equipment *(power supplies, geometry of the CT gantry, etc.)*, it appeared to be infeasible to use a conventional tungsten filament cathode structure for the EP tube design. For this reason, the initial design of the electron gun was performed by using standard **Pierce Gun** formulas *(reference-*[8]*)*.

The initial design of the gun mounted into the X-ray tube with an incident angle, α, of 10 degrees and an azimuthal angle, φ, of zero degrees is shown in Figure 11. Note that the X-ray anode *(or target)* is indented towards the center in order to have enough clearance for high voltage stability: a clearance of 0.5 inches (12 mm) is considered to be a minimum separation for a potential difference of 150 kV. Figure 12 shows the initial gun design with dimensions that provide the input into the computer program as a first trial for evaluating the properties of the gun and reshaping it to achieve an optimum electron beam cross section. The computer program was developed by Dr. W. B. Herrmannsfeld of SLAC, Stanford University, and has become an industry standard. Dr. Herrmannsfeld has recently developed a PC version of the code, which was used in the present evaluation.

Although the present application is truly of a three dimensional nature, the design can effectively be accomplished using the Herrmannsfeld two dimensional code. The classical **Pierce Gun** theory used for a first cut design does not include electron lenses beyond the first electrode, here called the **focussing electrode**. In the application to an X-ray tube, the

high voltage at the target generates a convergent electron lens resulting in a strong focussing effect on the electron beam. By modifying the electrode shapes, the strength of this lens may be considerably reduced to achieve a reasonable beam diameter at the target. Based on the computer evaluations, the final re-shaped gun design is shown in Figure 13, and the gun mounted in the X-ray tube is shown in figure 14. The dispenser cathode design shown in Figure 14 was examined and approved by Dr. Jim Cronin of Spectramat (Watsonville, CA), a company that specializes in the design and manufacturing of dispenser cathodes. The two major changes in the initial configuration are (a) the reshaping of the focussing electrode to minimize the lens effect, and (b) a smaller radius for the electron emitting surface, which was reduced from 0.3 to 0.2 inches. The intent of the electron gun optimization process is to require only one focussing electrode to focus the beam into the desired shape and size. A comparison of the initial and final electron gun design is shown in Figure 15. The configuration of the final gun design within the tube structure, which is used in the final computer analysis, is shown in Figure 16.

Figure 17 shows the result of the computer analysis, at a focusing electrode voltage of 8kV and a tube (target) voltage of 140kV. this tube voltage is typical for most CT scanner applications. The electron beam current is 480 mA, which is more than twice the maximum current used in standard tubes, as specified for the EP tube current requirement in Table 1. The emitting area of the gun is 0.2 cm^2, which results in a required emission current density of 2.4 A/cm^2, well within the range of modern dispenser cathodes, which are capable of 5 to 15 A/cm^2. The resulting focal spot as projected along the central beam is approximately 1.2 by 1.1 mm, which is a very typical focal spot as use din radiological practice. The kilovoltages for the focussing electrode and the target (8 kV / 140 kV, are given at the bottom of Figure 17. Equipotential curves shown are spaced in the following manner: (F = focusing voltage, T = target voltage, both in kV):

In the gun region: .1F, .3F, .5F, . . . 1.7F
In the region between gun and target: .2T, .4T, .6T, .8T

The axis numericals are in .01 inches, e.g. "24" means .240 inches. The scale is approximately 5:1.

Additional computer plots of electron beam trajectories similar to figure 17, were made for the following kilovoltages at the focussing electrode and target:

Focussing Electrode Kilovoltage: 3, 5, 8, 10 kV
Target Kilovoltage: 100, 120, 140, 150 kV

An approximate electron beam intensity distribution was developed for one typical case (5kV/150kV) and is shown in Figure 18. Compared to

conventional filament cathodes, the e-beam distribution is much more uniform than in the conventional case. Note particularly the sharp edges of the beam, which will result in very improved imaging performance compared to conventional filament gun designs.

The beam current increases approximately linearly with the focusing voltage, as shown in the following table:

focusing voltage (kV)	3	5	8	10
beam current (mA)	110	170	270	340

The computer generated electron trajectories, equipotential curves, and electron beam shape, is given in Figure 19 at a focusing voltage of 10kV and a target voltage of 150kV. The focal spot size stays nearly constant over the range of kV combinations, within 10%. This behavior represents an important advantage of this new gun design over the conventional gun optics used in Standard Tubes where there is a considerable increase in the focal spot sizes with increasing beam current *(the "blooming" effect).*

Based on the above results, the design of all the components of the electron gun was completed and is described in detail in Figures 20 to 25.

B. Design of the Complete EP Rotating Anode X-ray Tube.

The key feature of this enhanced power tube is the modified geometry and gun design which was carried out by Dr. Martin Braun as described in the previous sections. To complete the tube design, it is necessary to incorporate the gun design into a tube structure which contains the rotating anode and the tube envelope. Because Dr. Braun has recently designed and constructed a state-of-the-art metal ceramic rotating anode X-ray tube with the Standard geometry specified in Table 5, it was decided to combine the EP gun geometry with this improved ceramic tube structure to obtain a final tube design which would have superior properties over all present day rotating anode X-ray tubes.

The ceramic rotating anode tube previously constructed by Dr. Braun with the Standard geometry is shown in Figure 26. Compared to the glass envelope, oil-cooled, rotating anode tube, this new ceramic tube has the following advantages:

a. Compact, metal ceramic construction
b. Oil cooling system eliminated, replaced by air cooling of ceramic housing

c. Bearings are "straddle" mounted, thus there is less rotor wobble and less bearing load and wear
d. Shaft ceramic insulates rotor allowing efficient electrical coupling
e. Geometrical precision not achievable with glass
f. Reduced off-focus radiation
h. Motor stator is easily installed
i. Simple tube housing *(no oil leaks or oil expansion)*
j. Can reuse many components when tube fails

A sample design of the new EP tube which combines the new EP geometry and the new air-cooled rotating anode ceramic tube structure is shown in Figure 27, with the initial gun electrode design. This new EP tube promises to have the following important advantages over all present-day rotating anode tubes:

* Enhanced X-ray power output ranging from a factor of 1.6 at 150 Kilovolts to 2.4 at 500 Kilovolts.

* Oil cooling system replaced by air cooling of ceramic housing.

* Bearings are "straddle" mounted with less rotor wobble and less bearing load and wear.

* Compact metal ceramic construction with geometrical precision not achievable with glass.

* Reduced off-focus radiation.

* Longer tube life (2 to 4 times longer)

* Less down time (tube replacement cycle of .5 days versus 1.5 days).

References

[1] G. J. Lockwood, L. E. ruggles, G. H. Miller, J. A. Halbleib, **"Electron energy and Charge Albedos - Calorimetric Measurement vs Monte Carlo Theory"**, Sandia Report SAND 80-1968 U.C. - 34a November 1981, Sandie National Laboratories, Albuquerque, New Mexico, 87185.

[2] M. J. Berger, **"Monte Carlo Calculations of the Penetration and Diffusion of Fast Charged Particles"**, in Methods of Computational Physics, Vol. 1, ed. by B. Alder, S. Fernbach and M. Rotenberg. (Academic Press, New York, 1963).

[3] S. M. Seltzer, **"An Overview of ETRAN Monte Carlo Methods"**, pp 153 - 181 in Monte Carlo Transport of Electrons and Photons, ed. by Thomas M. Jenkins, W. R. Nelson and A. Rindi. (Plenum Press, New York, 1988).

[4] M. J. Berger, **"Etran - Experimental Benchmarks"**, pp 183 - 219, ibidem.

[5] J. Halbleib, **"Applications of the ITS Codes"**, pp 263 - 284, ibidem.

[6] S. M. Seltzer and M. J. Berger, **"Bremsstrahlung Spectra from Electron Interactions with Screened Atomic Nuclei and Orbital Electrons"**, Nucl. Instr. Meth. B12, 95 (1985); and **"Bremsstrahlung Energy Spectra from Electrons with Kinetic Energy 1 keV - 100 GeV Incident on Screened Nuclei and orbital Electrons of Neutral Atoms with Z = 1 - 100"**, Atom. and Nuclear Data Tables 35, 345 (1986).

[7] M. J. Berger and J. H Hubbell, **"XCOM: Photon Cross Sections on a Personal Computer"**, National Bureau of Standards Report NBSIR 87-3597 (1987).

[8] J.R.M. Vaughan, "Synthesis of the Pierce Gun", IEEE Trans El Dev, ED-28, Jan 1981.

Table 1. Evaluation of $N(k,\theta)$

T = energy of incident electron (keV)
Alpha = angle of incidence (deg)
Theta = angle of emergence of photons (deg)
k = photon spectral energy (keV)

Alpha	T
90.0	150.0

PHOTON FLUX SPECTRUM (per keV and unit solid angle), averaged over azimuths between -10 and +10 degrees, and over indicated theta (obliquity-angle) intervals

Note that the histogram bins marked with (*) contain characteristic K x-rays with energies of 67.25, 59.32 and 57.98 keV, respectively.

k	Theta =	0 - 5	5 - 10	10 - 15	15 - 20	20 - 25	25 - 30	30 - 35	35 - 40	40 - 45
	150.0 - 145.0	2.65E-07	1.39E-04	3.17E-04	2.55E-04	1.50E-04	7.82E-05	2.89E-04	4.41E-05	4.73E-05
	145.0 - 140.0	4.26E-07	5.45E-04	4.21E-04	3.61E-04	4.12E-04	4.31E-04	2.88E-04	3.07E-04	3.30E-04
	140.0 - 135.0	7.30E-07	1.01E-03	1.18E-03	6.85E-04	4.88E-04	6.24E-04	4.91E-04	6.13E-04	5.64E-04
	135.0 - 130.0	1.07E-06	1.17E-03	1.49E-03	1.40E-03	1.23E-03	1.01E-03	1.51E-03	7.42E-04	7.08E-04
	130.0 - 125.0	1.12E-06	1.84E-03	1.73E-03	1.43E-03	1.34E-03	1.40E-03	1.76E-03	8.30E-04	1.55E-03
	125.0 - 120.0	1.34E-06	1.60E-03	2.03E-03	1.66E-03	1.88E-03	1.46E-03	1.70E-03	1.43E-03	1.87E-03
	120.0 - 115.0	1.59E-06	2.00E-03	1.99E-03	2.04E-03	2.42E-03	2.12E-03	2.18E-03	2.20E-03	1.87E-03
	115.0 - 110.0	1.88E-06	3.14E-03	2.56E-03	2.63E-03	2.36E-03	2.72E-03	2.15E-03	2.06E-03	2.41E-03
	110.0 - 105.0	2.17E-06	2.85E-03	3.07E-03	3.04E-03	2.87E-03	3.42E-03	2.74E-03	2.79E-03	2.84E-03
	105.0 - 100.0	2.08E-06	3.66E-03	3.55E-03	3.52E-03	3.84E-03	3.87E-03	3.69E-03	3.45E-03	3.61E-03
	100.0 - 95.0	2.46E-06	4.33E-03	4.52E-03	3.50E-03	4.00E-03	4.77E-03	3.85E-03	4.04E-03	3.47E-03
	95.0 - 90.0	2.77E-06	4.47E-03	5.01E-03	4.42E-03	4.99E-03	4.60E-03	4.52E-03	4.23E-03	4.77E-03
	90.0 - 85.0	3.06E-06	5.07E-03	5.47E-03	5.77E-03	5.84E-03	5.79E-03	5.70E-03	5.36E-03	5.82E-03
	85.0 - 80.0	3.06E-06	5.72E-03	5.03E-03	5.00E-03	6.76E-03	6.84E-03	6.64E-03	5.87E-03	6.26E-03
	80.0 - 75.0	3.48E-06	5.48E-03	6.51E-03	6.72E-03	6.98E-03	7.08E-03	7.00E-03	6.67E-03	6.53E-03
	75.0 - 70.0	3.20E-06	5.70E-03	7.37E-03	7.67E-03	7.58E-03	7.64E-03	8.54E-03	9.11E-03	7.49E-03
	70.0 - 67.3	6.94E-06	1.03E-02	9.51E-03	1.09E-02	8.93E-03	9.57E-03	1.08E-02	8.01E-03	7.79E-03
*	67.3 - 67.2	1.91E-04	2.66E-01	3.63E-01	3.74E-01	3.50E-01	3.93E-01	3.44E-01	5.11E-01	4.18E-01
	67.2 - 65.0	6.31E-06	9.20E-03	1.07E-02	1.16E-02	1.28E-02	1.05E-02	1.03E-02	1.12E-02	8.64E-03
	65.0 - 60.0	7.87E-06	1.09E-02	1.19E-02	1.16E-02	1.23E-02	1.16E-02	1.19E-02	1.10E-02	1.19E-02
	60.0 - 59.4	9.04E-06	1.10E-02	1.10E-02	1.20E-02	1.23E-02	1.13E-02	1.33E-02	1.32E-02	1.42E-02
*	59.4 - 59.3	3.39E-04	5.57E-01	6.80E-01	6.57E-01	6.01E-01	6.41E-01	6.06E-01	6.36E-01	9.36E-01
	59.3 - 58.0	9.46E-06	1.33E-02	1.35E-02	1.46E-02	1.18E-02	1.38E-02	1.53E-02	1.20E-02	1.12E-02
*	58.0 - 57.9	2.02E-04	3.45E-01	3.46E-01	4.14E-01	4.62E-01	5.13E-01	4.07E-01	3.35E-01	4.88E-01
	57.9 - 55.0	7.44E-06	1.19E-02	1.38E-02	1.36E-02	1.37E-02	1.25E-02	1.29E-02	1.38E-02	1.40E-02
	55.0 - 50.0	8.20E-06	1.36E-02	1.53E-02	1.47E-02	1.71E-02	1.52E-02	1.50E-02	1.46E-02	1.33E-02
	50.0 - 45.0	8.45E-06	1.54E-02	1.64E-02	1.77E-02	1.86E-02	1.70E-02	1.82E-02	1.92E-02	1.85E-02
	45.0 - 40.0	8.26E-06	1.45E-02	1.70E-02	1.93E-02	1.90E-02	2.09E-02	2.10E-02	1.94E-02	2.15E-02
	40.0 - 35.0	7.76E-06	1.63E-02	2.04E-02	2.20E-02	2.24E-02	2.21E-02	2.39E-02	2.42E-02	2.54E-02
	35.0 - 30.0	6.31E-06	1.66E-02	2.04E-02	2.27E-02	2.55E-02	2.59E-02	2.86E-02	2.74E-02	3.03E-02
	30.0 - 25.0	5.63E-06	1.52E-02	2.10E-02	2.56E-02	2.69E-02	3.00E-02	3.08E-02	3.40E-02	3.20E-02
	25.0 - 20.0	3.73E-06	1.29E-02	1.96E-02	2.47E-02	2.71E-02	3.20E-02	3.28E-02	3.44E-02	3.54E-02
	20.0 - 15.0	2.30E-06	7.90E-03	1.41E-02	1.84E-02	2.39E-02	2.62E-02	2.96E-02	3.31E-02	3.46E-02
	15.0 - 10.0	1.65E-06	5.61E-03	1.05E-02	1.42E-02	1.88E-02	2.21E-02	2.60E-02	2.67E-02	3.11E-02

Table 1. (Continued)

T = energy of incident electron (keV)
Alpha = angle of incidence (deg)
Theta = angle of emergence of photons (deg)
k = photon spectral energy (keV)

Alpha	T
90.0	150.0

PHOTON FLUX SPECTRUM (per keV and unit solid angle), averaged over azimuths between -10 and +10 degrees, and over indicated theta (obliquity-angle) intervals

Note that the histogram bins marked with (*) contain characteristic K x-rays with energies of 67.25, 59.32 and 57.98 keV, respectively.

k \ Theta =	45 50	50 55	55 60	60 65	65 70	70 75	75 80	80 85	85 90
150.0 - 145.0	0.00E+00	1.14E-04	1.29E-04	7.58E-05	0.00E+00	1.16E-04	0.00E+00	0.00E+00	0.00E+00
145.0 - 140.0	5.15E-04	3.44E-04	5.19E-04	2.27E-04	1.82E-04	3.48E-04	0.00E+00	2.67E-04	8.01E-04
140.0 - 135.0	5.16E-04	5.72E-04	4.53E-04	4.53E-04	5.45E-04	3.48E-04	4.83E-04	1.07E-03	8.00E-04
135.0 - 130.0	6.14E-04	6.83E-04	6.71E-04	5.89E-04	6.18E-04	1.04E-03	4.83E-04	0.00E+00	7.98E-04
130.0 - 125.0	1.43E-03	1.93E-03	1.36E-03	9.76E-04	9.09E-04	6.93E-04	9.52E-04	7.92E-04	1.59E-03
125.0 - 120.0	1.23E-03	1.19E-03	1.16E-03	1.78E-03	1.27E-03	2.08E-03	1.12E-03	2.13E-03	2.38E-03
120.0 - 115.0	1.99E-03	1.82E-03	2.25E-03	1.42E-03	1.26E-03	2.07E-03	8.00E-04	2.39E-03	1.59E-03
115.0 - 110.0	2.46E-03	2.43E-03	2.71E-03	1.80E-03	1.98E-03	1.95E-03	1.28E-03	1.84E-03	1.59E-03
110.0 - 105.0	3.07E-03	2.54E-03	2.90E-03	2.01E-03	3.07E-03	2.67E-03	3.18E-03	2.63E-03	7.99E-04
105.0 - 100.0	2.49E-03	2.95E-03	3.23E-03	3.42E-03	3.24E-03	3.30E-03	3.49E-03	3.30E-03	6.31E-03
100.0 - 95.0	4.44E-03	4.12E-03	4.17E-03	3.91E-03	4.10E-03	3.07E-03	4.58E-03	4.45E-03	7.58E-03
95.0 - 90.0	5.20E-03	4.12E-03	3.70E-03	4.44E-03	3.87E-03	4.49E-03	4.30E-03	2.55E-03	4.33E-03
90.0 - 85.0	5.17E-03	5.13E-03	6.06E-03	5.07E-03	5.31E-03	5.12E-03	6.73E-03	6.58E-03	4.64E-03
85.0 - 80.0	6.73E-03	5.69E-03	5.89E-03	5.26E-03	6.06E-03	5.89E-03	6.42E-03	4.98E-03	5.31E-03
80.0 - 75.0	6.87E-03	7.47E-03	6.35E-03	8.39E-03	6.94E-03	6.19E-03	5.93E-03	5.74E-03	1.01E-02
75.0 - 70.0	8.29E-03	8.00E-03	8.46E-03	7.80E-03	8.34E-03	7.98E-03	7.92E-03	6.95E-03	6.63E-03
70.0 - 67.3	8.93E-03	9.03E-03	9.34E-03	1.03E-02	8.62E-03	9.90E-03	1.02E-02	6.11E-03	7.44E-03
* 67.3 - 67.2	3.88E-01	4.61E-01	3.96E-01	2.99E-01	2.90E-01	5.15E-01	4.04E-01	4.28E-01	4.53E-01
67.2 - 65.0	9.78E-03	9.96E-03	1.02E-02	1.06E-02	1.08E-02	7.77E-03	1.05E-02	1.02E-02	7.20E-03
65.0 - 60.0	1.21E-02	1.19E-02	1.25E-02	1.15E-02	1.24E-02	9.67E-03	9.98E-03	9.68E-03	1.27E-02
60.0 - 59.4	9.26E-03	9.94E-03	1.59E-02	1.89E-02	9.24E-03	1.04E-02	1.78E-02	1.66E-02	6.60E-03
* 59.4 - 59.3	8.19E-01	1.06E+00	8.80E-01	9.81E-01	8.28E-01	7.97E-01	9.05E-01	1.36E+00	7.16E-01
59.3 - 58.0	1.51E-02	1.41E-02	1.65E-02	1.32E-02	1.01E-02	1.23E-02	7.94E-03	1.33E-02	2.17E-02
* 58.0 - 57.9	5.26E-01	5.13E-01	5.28E-01	4.45E-01	4.04E-01	4.59E-01	8.49E-01	4.42E-01	4.31E-01
57.9 - 55.0	1.64E-02	1.37E-02	1.51E-02	1.53E-02	1.51E-02	1.30E-02	1.86E-02	1.63E-02	2.17E-02
55.0 - 50.0	1.86E-02	1.78E-02	1.68E-02	1.67E-02	2.12E-02	1.63E-02	1.94E-02	1.66E-02	1.54E-02
50.0 - 45.0	1.66E-02	1.90E-02	1.91E-02	1.88E-02	1.71E-02	1.74E-02	1.94E-02	1.93E-02	2.63E-02
45.0 - 40.0	1.84E-02	2.13E-02	2.34E-02	2.11E-02	2.22E-02	2.05E-02	2.08E-02	2.47E-02	2.13E-02
40.0 - 35.0	2.45E-02	2.46E-02	2.37E-02	2.70E-02	2.53E-02	2.48F-02	2.46E-02	2.74E-02	3.02E-02
35.0 - 30.0	2.90E-02	2.70E-02	2.83E-02	2.84E-02	3.01E-02	2.80E-02	2.70E-02	2.86E-02	3.39E-02
30.0 - 25.0	3.00E-02	3.28E-02	3.49E-02	3.18E-02	3.21E-02	3.28E-02	3.70E-02	3.37E-02	3.13E-02
25.0 - 20.0	3.64E-02	3.58E-02	3.88E-02	3.86E-02	3.95E-02	3.64E-02	4.39E-02	3.74E-02	4.16E-02
20.0 - 15.0	3.61E-02	3.73E-02	3.65E-02	4.12E-02	3.79E-02	3.93E-02	4.00E-02	4.27E-02	3.71E-02
15.0 - 10.0	3.30E-02	3.54E-02	3.91E-02	3.99E-02	3.83E-02	4.02E-02	4.20E-02	4.62E-02	3.80E-02

Table 2. Evaluation of $E_x(\theta,\varphi)$

T(kev)	Alpha(deg)
150.0	90.0

INTEGRATED PHOTON ENERGY FLUX, keV per unit solid angle,
and per incident electron
(includes photons with energies above 10 keV)

Theta =	0	5	10	15	20	25	30	35	40
	5	10	15	20	25	30	35	40	45
Phi									
0 - 10	3.63E-05	6.12E-05	6.98E-05	7.35E-05	7.69E-05	7.84E-05	7.92E-05	7.80E-05	8.01E-05
10 - 20	3.72E-05	6.10E-05	6.78E-05	7.32E-05	7.53E-05	7.41E-05	7.63E-05	7.81E-05	7.93E-05
20 - 30	3.58E-05	5.94E-05	7.00E-05	7.12E-05	7.46E-05	7.55E-05	7.65E-05	7.73E-05	7.87E-05
30 - 40	3.71E-05	6.05E-05	6.74E-05	7.43E-05	7.72E-05	7.76E-05	7.56E-05	7.99E-05	7.91E-05
40 - 50	3.68E-05	6.14E-05	6.79E-05	7.36E-05	7.52E-05	7.80E-05	7.70E-05	7.78E-05	8.04E-05
50 - 60	3.77E-05	5.91E-05	6.85E-05	7.22E-05	7.71E-05	7.68E-05	7.88E-05	7.90E-05	7.94E-05
60 - 70	3.60E-05	6.11E-05	6.86E-05	7.29E-05	7.42E-05	7.68E-05	7.63E-05	8.13E-05	8.02E-05
70 - 80	3.71E-05	6.04E-05	6.83E-05	7.33E-05	7.80E-05	7.81E-05	7.85E-05	7.89E-05	8.18E-05
80 - 90	3.75E-05	6.14E-05	6.85E-05	7.26E-05	7.45E-05	7.63E-05	7.79E-05	7.87E-05	8.05E-05
90 - 100	3.65E-05	6.00E-05	6.92E-05	7.26E-05	7.48E-05	7.74E-05	7.96E-05	7.83E-05	8.02E-05
100 - 110	3.70E-05	6.01E-05	6.80E-05	7.40E-05	7.67E-05	7.74E-05	7.71E-05	7.85E-05	7.79E-05
110 - 120	3.65E-05	5.92E-05	6.83E-05	7.32E-05	7.32E-05	7.60E-05	7.77E-05	7.87E-05	7.81E-05
120 - 130	3.61E-05	6.11E-05	6.93E-05	7.23E-05	7.65E-05	7.85E-05	7.82E-05	7.73E-05	7.84E-05
130 - 140	3.66E-05	6.04E-05	7.04E-05	7.29E-05	7.47E-05	7.78E-05	7.86E-05	7.64E-05	7.94E-05
140 - 150	3.77E-05	6.00E-05	6.96E-05	7.41E-05	7.61E-05	7.58E-05	7.74E-05	8.04E-05	7.53E-05
150 - 160	3.63E-05	6.03E-05	6.98E-05	7.34E-05	7.65E-05	7.60E-05	7.91E-05	7.87E-05	7.97E-05
160 - 170	3.77E-05	5.82E-05	6.88E-05	7.24E-05	7.50E-05	7.70E-05	7.80E-05	7.88E-05	7.88E-05
170 - 180	3.64E-05	6.07E-05	7.01E-05	7.14E-05	7.49E-05	7.58E-05	7.92E-05	8.06E-05	8.17E-05

Theta =	45	50	55	60	65	70	75	80	85
	50	55	60	65	70	75	80	85	90
Phi									
0 - 10	8.06E-05	8.23E-05	8.35E-05	8.12E-05	8.02E-05	7.88E-05	8.47E-05	8.42E-05	8.80E-05
10 - 20	8.19E-05	7.72E-05	7.70E-05	7.71E-05	7.79E-05	7.54E-05	7.83E-05	8.19E-05	7.52E-05
20 - 30	7.90E-05	7.93E-05	7.97E-05	7.92E-05	7.84E-05	8.12E-05	8.31E-05	7.70E-05	8.31E-05
30 - 40	8.02E-05	7.96E-05	7.76E-05	7.68E-05	7.48E-05	7.74E-05	8.33E-05	7.72E-05	8.39E-05
40 - 50	7.98E-05	7.84E-05	7.97E-05	7.93E-05	7.54E-05	7.80E-05	8.19E-05	8.25E-05	7.62E-05
50 - 60	7.84E-05	7.87E-05	7.86E-05	7.74E-05	7.71E-05	7.97E-05	8.02E-05	7.60E-05	7.68E-05
60 - 70	7.85E-05	7.92E-05	8.05E-05	7.78E-05	8.12E-05	7.98E-05	7.89E-05	8.31E-05	7.98E-05
70 - 80	7.82E-05	8.05E-05	7.76E-05	7.86E-05	7.88E-05	8.05E-05	7.98E-05	7.87E-05	8.09E-05
80 - 90	8.01E-05	7.93E-05	7.93E-05	8.09E-05	7.84E-05	7.97E-05	7.84E-05	8.20E-05	7.45E-05
90 - 100	7.98E-05	7.71E-05	7.58E-05	7.62E-05	7.85E-05	8.02E-05	7.88E-05	8.35E-05	8.08E-05
100 - 110	8.17E-05	8.01E-05	7.81E-05	7.97E-05	7.92E-05	8.37E-05	7.81E-05	7.98E-05	8.31E-05
110 - 120	7.90E-05	7.79E-05	7.61E-05	8.01E-05	8.12E-05	7.88E-05	8.06E-05	7.27E-05	8.01E-05
120 - 130	8.01E-05	7.97E-05	7.77E-05	7.85E-05	7.79E-05	8.11E-05	7.80E-05	7.03E-05	8.40E-05
130 - 140	7.68E-05	8.30E-05	7.92E-05	7.64E-05	7.73E-05	8.04E-05	8.16E-05	7.74E-05	7.72E-05
140 - 150	7.98E-05	7.85E-05	7.81E-05	7.77E-05	7.88E-05	8.01E-05	7.67E-05	7.41E-05	7.46E-05
150 - 160	7.69E-05	7.68E-05	8.05E-05	7.76E-05	7.78E-05	7.91E-05	7.75E-05	7.97E-05	7.68E-05
160 - 170	7.72E-05	8.12E-05	7.94E-05	7.58E-05	7.90E-05	7.99E-05	8.25E-05	8.05E-05	9.05E-05
170 - 180	8.19E-05	8.13E-05	8.30E-05	8.03E-05	8.65E-05	8.50E-05	8.21E-05	8.72E-05	8.16E-05

Table 3. Evaluation of $E_{T'}/E_T$, Ex/E_T, E_D, and Ex/E_D

Incident electron energy T = 150.0 (keV)

ALPHA	$E_{T'}/E_T$	Ex/E_T	E_D	Ex/E_D
90	.4103	3.009E-03	88.00	3.42E-05
70	.4282	2.944E-03	85.33	3.45E-05
50	.4786	2.755E-03	77.80	3.54E-05
30	.5695	2.367E-03	64.22	3.69E-05
20	.6328	2.063E-03	54.77	3.77E-05
10	.7161	1.622E-03	42.34	3.83E-05
5	.7669	1.336E-03	34.76	3.84E-05
2	.8002	1.145E-03	29.80	3.84E-05

Incident electron energy T = 150.0 (keV) = E_T for one electron

Alpha = angle of incidence of electron (deg)

$E_{T'}/E_T$ = electron energy albedo

E_D = energy absorbed in target (keV)

$E_D = E_T (1 - E_{T'}/E_T - Ex/E_T)$

Table 4. Evaluation of $E_X(\theta)$ and $E_X(\theta) / E_D$

Alpha = angle of incidence of electron (deg)
Theta = angle of emergence of x-ray photons (deg)
$E_X(\theta)$ = integrated photon energy flux, keV per unit solid angle
averaged over azimuths from -10 to +10 deg,
integrated over all energies above cutoff
E_D = energy deposited in target (keV)

Incident electron energy T = 100.0 (keV)
(Energy cutoff 10 keV)

$E_X(\theta)$

Theta	ALPHA = 90	70	50	30	20	10	5	2
0 - 5	1.77E-02	1.93E-02	2.06E-02	2.03E-02	1.86E-02	1.57E-02	1.29E-02	1.14E-02
5 - 10	2.74E-02	2.95E-02	2.96E-02	2.92E-02	2.59E-02	2.13E-02	1.73E-02	1.47E-02
10 - 15	3.10E-02	3.28E-02	3.39E-02	3.08E-02	2.80E-02	2.32E-02	1.86E-02	1.58E-02
15 - 20	3.19E-02	3.34E-02	3.31E-02	3.16E-02	2.90E-02	2.36E-02	1.93E-02	1.64E-02
20 - 25	3.35E-02	3.46E-02	3.38E-02	3.27E-02	2.91E-02	2.36E-02	1.96E-02	1.68E-02
25 - 30	3.49E-02	3.49E-02	3.58E-02	3.23E-02	2.89E-02	2.36E-02	1.89E-02	1.65E-02
30 - 35	3.45E-02	3.58E-02	3.52E-02	3.21E-02	2.88E-02	2.37E-02	2.00E-02	1.73E-02
35 - 40	3.57E-02	3.57E-02	3.42E-02	3.19E-02	2.80E-02	2.27E-02	1.88E-02	1.61E-02
40 - 45	3.61E-02	3.61E-02	3.42E-02	3.07E-02	2.81E-02	2.32E-02	1.88E-02	1.62E-02
45 - 50	3.49E-02	3.53E-02	3.40E-02	3.01E-02	2.72E-02	2.18E-02	1.80E-02	1.51E-02
50 - 55	3.57E-02	3.52E-02	3.35E-02	2.94E-02	2.65E-02	2.07E-02	1.72E-02	1.50E-02
55 - 60	3.55E-02	3.46E-02	3.31E-02	3.01E-02	2.59E-02	2.08E-02	1.69E-02	1.47E-02
60 - 65	3.60E-02	3.49E-02	3.35E-02	2.92E-02	2.56E-02	2.11E-02	1.74E-02	1.43E-02
65 - 70	3.59E-02	3.62E-02	3.32E-02	2.89E-02	2.56E-02	2.07E-02	1.63E-02	1.43E-02
70 - 75	3.37E-02	3.50E-02	3.32E-02	2.82E-02	2.49E-02	1.95E-02	1.58E-02	1.31E-02
75 - 80	3.55E-02	3.66E-02	3.36E-02	2.87E-02	2.42E-02	1.91E-02	1.67E-02	1.45E-02
80 - 85	3.49E-02	3.52E-02	3.29E-02	2.85E-02	2.38E-02	1.74E-02	1.55E-02	1.26E-02
85 - 90	3.22E-02	3.50E-02	3.37E-02	2.49E-02	1.98E-02	1.80E-02	1.54E-02	1.24E-02

RATIO OF INTEGRATED PHOTON ENERGY FLUX TO DEPOSITED ENERGY $= E_X(\theta) / E_D$

Theta	ALPHA = 90	70	50	30	20	10	5	2
0 - 5	2.88E-04	3.23E-04	3.79E-04	4.50E-04	4.83E-04	5.23E-04	5.25E-04	5.43E-04
5 - 10	4.46E-04	4.94E-04	5.44E-04	6.47E-04	6.73E-04	7.09E-04	7.04E-04	7.00E-04
10 - 15	5.05E-04	5.49E-04	6.24E-04	6.82E-04	7.27E-04	7.73E-04	7.57E-04	7.53E-04
15 - 20	5.19E-04	5.59E-04	6.09E-04	7.00E-04	7.53E-04	7.86E-04	7.86E-04	7.81E-04
20 - 25	5.45E-04	5.79E-04	6.22E-04	7.24E-04	7.56E-04	7.86E-04	7.98E-04	8.00E-04
25 - 30	5.68E-04	5.84E-04	6.59E-04	7.16E-04	7.50E-04	7.86E-04	7.70E-04	7.86E-04
30 - 35	5.62E-04	5.99E-04	6.47E-04	7.11E-04	7.48E-04	7.89E-04	8.14E-04	8.24E-04
35 - 40	5.81E-04	5.98E-04	6.29E-04	7.07E-04	7.27E-04	7.56E-04	7.66E-04	7.67E-04
40 - 45	5.88E-04	6.04E-04	6.29E-04	6.80E-04	7.30E-04	7.73E-04	7.66E-04	7.72E-04
45 - 50	5.68E-04	5.91E-04	6.25E-04	6.67E-04	7.06E-04	7.26E-04	7.33E-04	7.19E-04
50 - 55	5.81E-04	5.89E-04	6.16E-04	6.51E-04	6.88E-04	6.89E-04	7.00E-04	7.15E-04
55 - 60	5.78E-04	5.79E-04	6.09E-04	6.67E-04	6.73E-04	6.93E-04	6.88E-04	7.00E-04
60 - 65	5.86E-04	5.84E-04	6.16E-04	6.47E-04	6.65E-04	7.03E-04	7.09E-04	6.81E-04
65 - 70	5.85E-04	6.06E-04	6.11E-04	6.40E-04	6.65E-04	6.89E-04	6.64E-04	6.81E-04
70 - 75	5.49E-04	5.86E-04	6.11E-04	6.25E-04	6.47E-04	6.49E-04	6.43E-04	6.24E-04
75 - 80	5.78E-04	6.13E-04	6.18E-04	6.36E-04	6.28E-04	6.36E-04	6.80E-04	6.91E-04
80 - 85	5.68E-04	5.89E-04	6.05E-04	6.31E-04	6.18E-04	5.79E-04	6.31E-04	6.00E-04
85 - 90	5.24E-04	5.86E-04	6.20E-04	5.52E-04	5.14E-04	5.99E-04	6.27E-04	5.91E-04

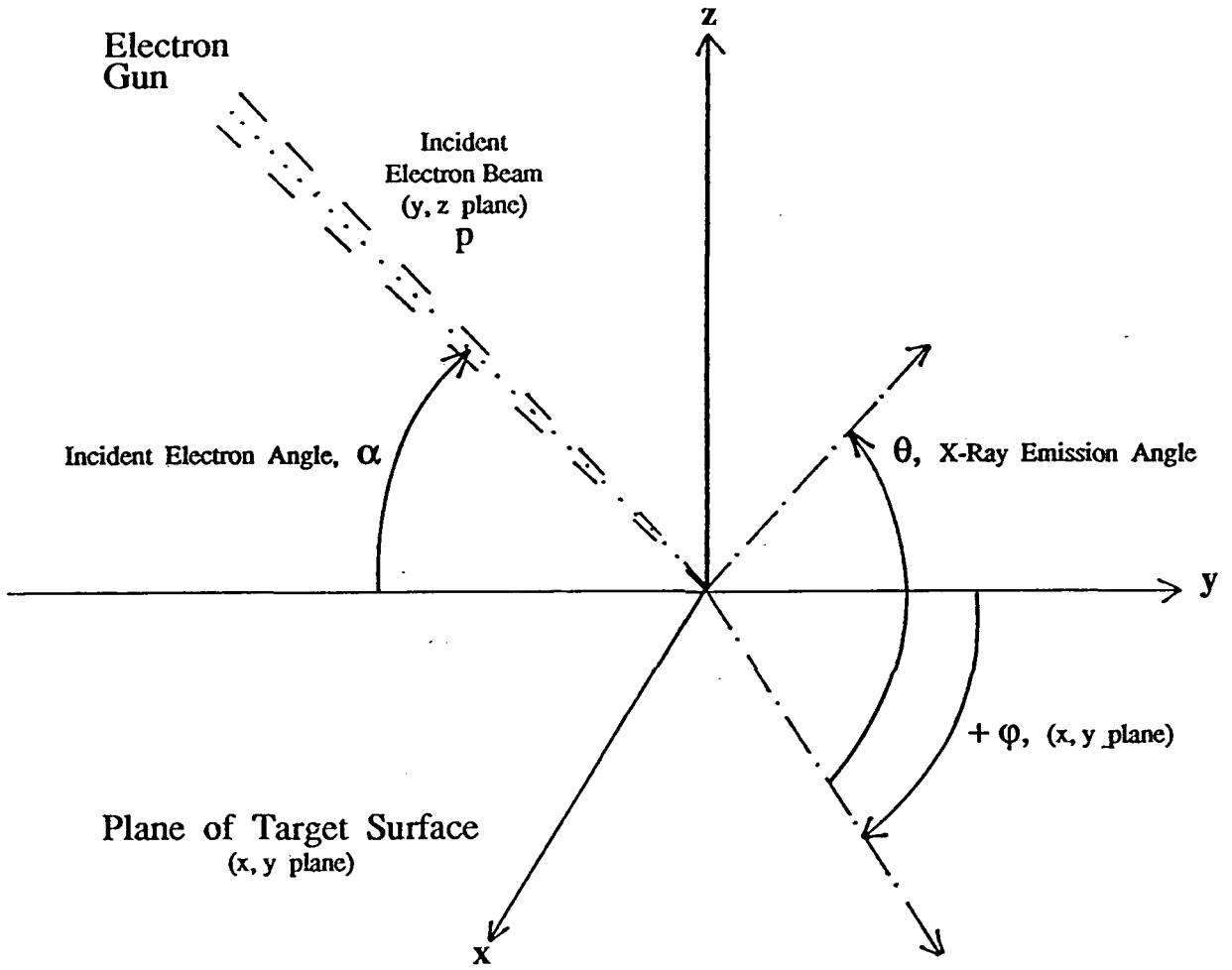

Figure 1. Geometric parameters for the x-ray tube. The incident plane *(***p**, **z***)* is defined by the electron momentum vector, **p**, and the vector, **z**, normal to the plane of the target surface (**x**, **y**). The emission plane *(***k**, **z***)* is defined by the photon momentum vector, **k**, and the vector **z**. The remaining parameters include the incident angle, α, the emission angle, θ, and the azimuthal angle, φ, between the incident and emission planes as described above.

Figure 2. Dependence of the X-ray energy emission ratio, E_X / E_T, on the incident electron angle, α, for electron energies, T, equal to 50, 100, 150, 200, 300, 400, and 500 keV.

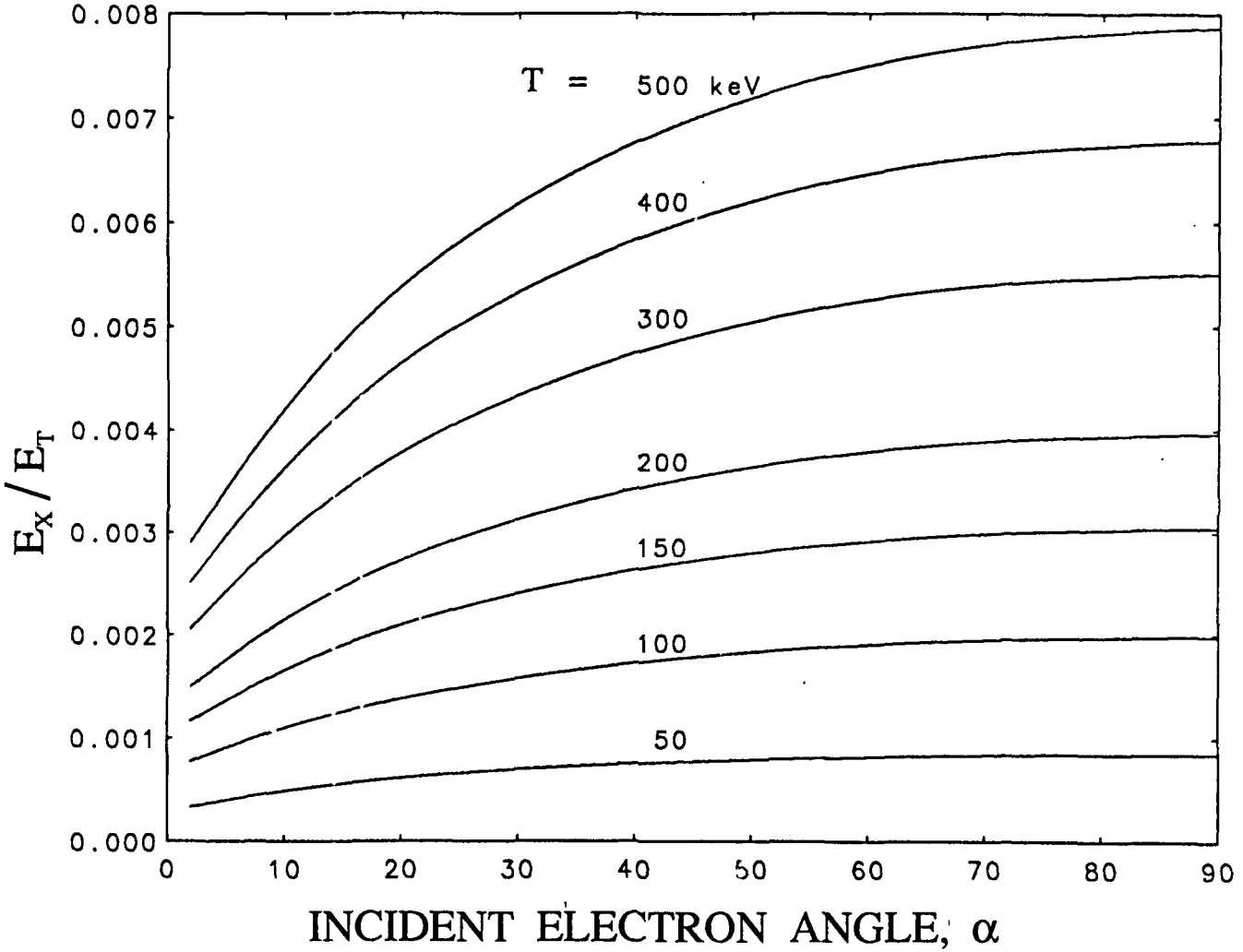

Figure 3. Dependence of $E_x(\theta)$ on the X-ray emission angle, θ, for incident electron angles, α, of 10 and 70 degrees, at 150 kilovolts.

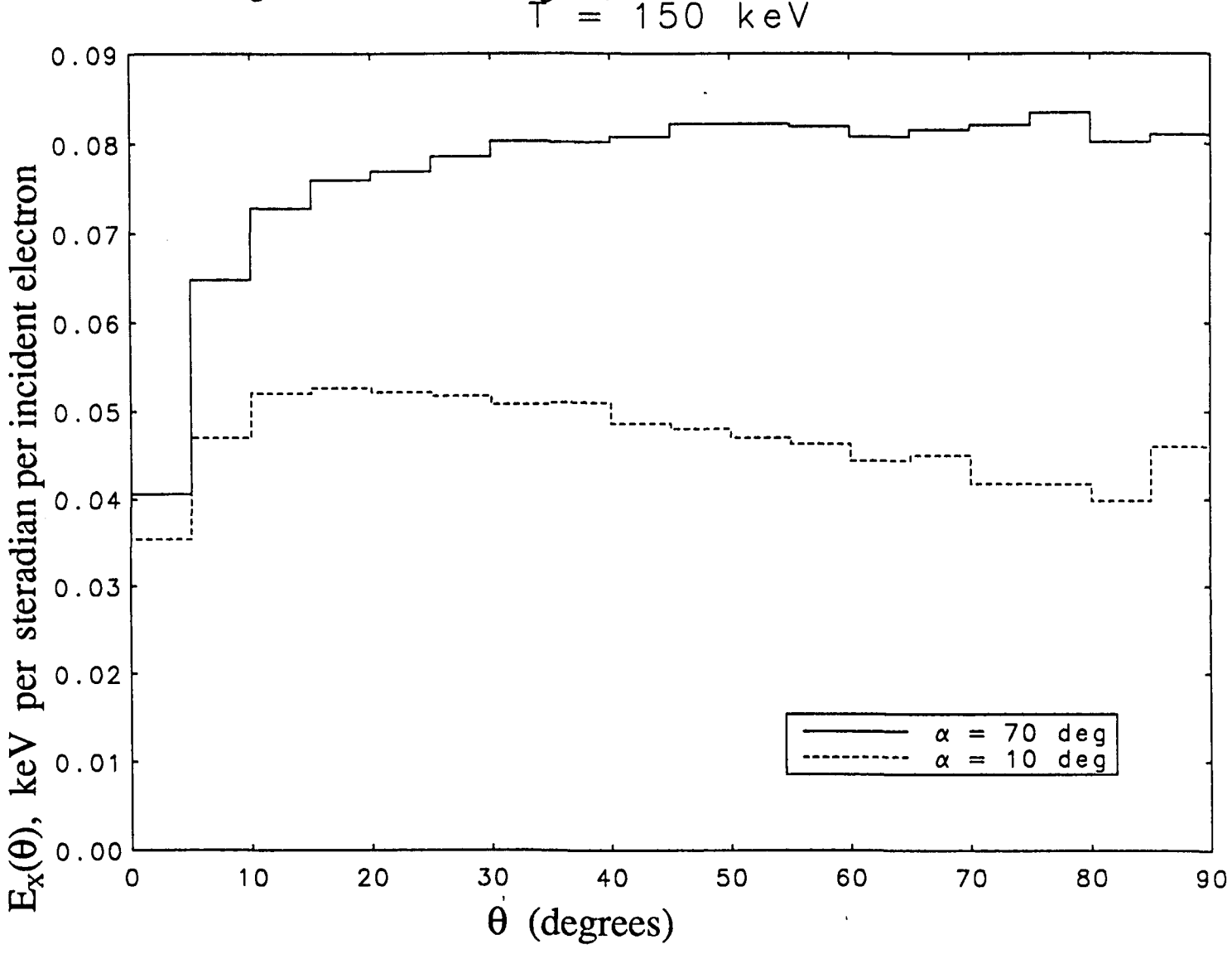

Figure 4. Dependence of $E_X(\theta)$ on α, for incident electron energies of 50, 150, and 500 keV

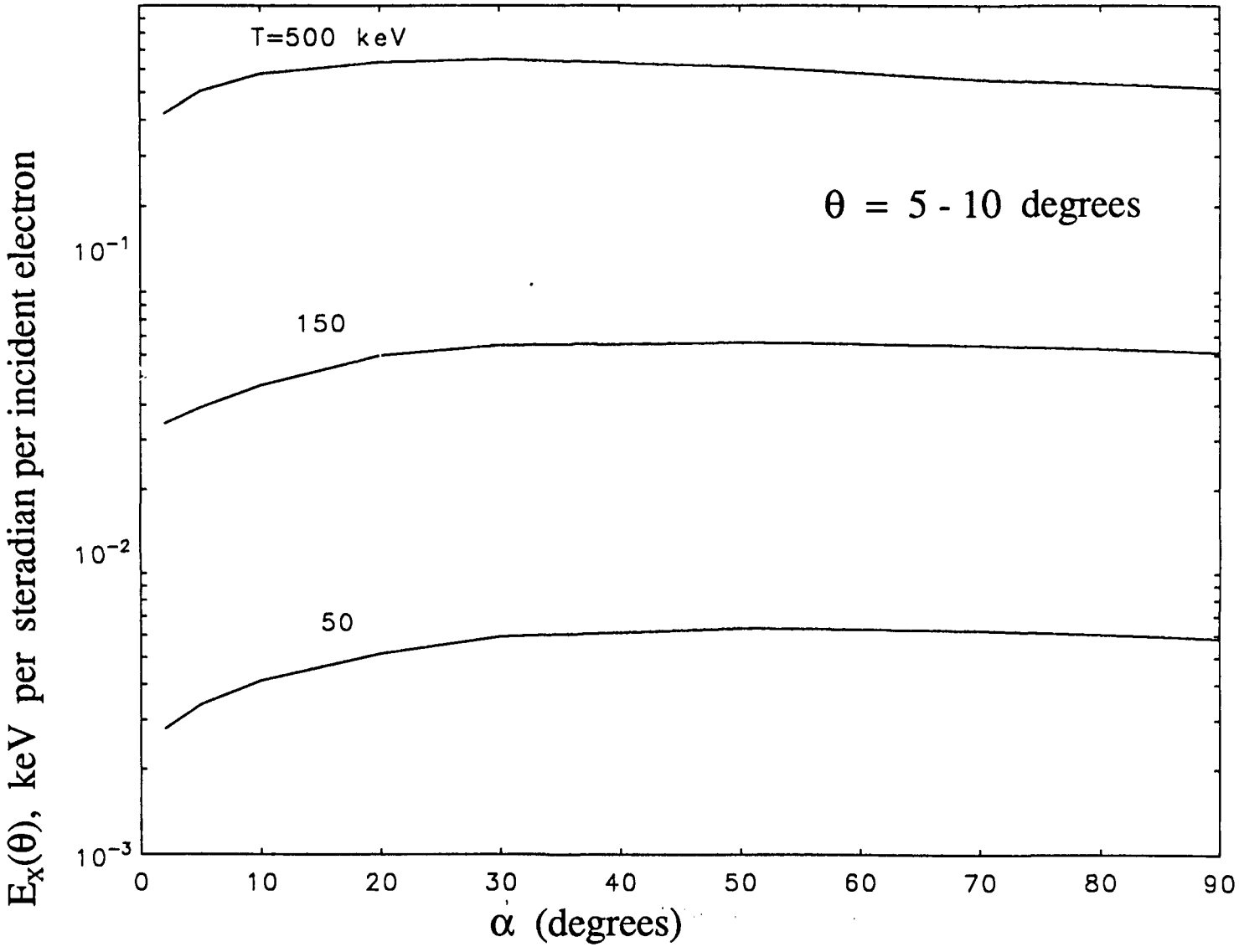

Figure 5. Dependence of the electron deposition energy fraction, E_D / E_T, on the incident electron angle, α, for incident electron energies of 100 and 500 keV.

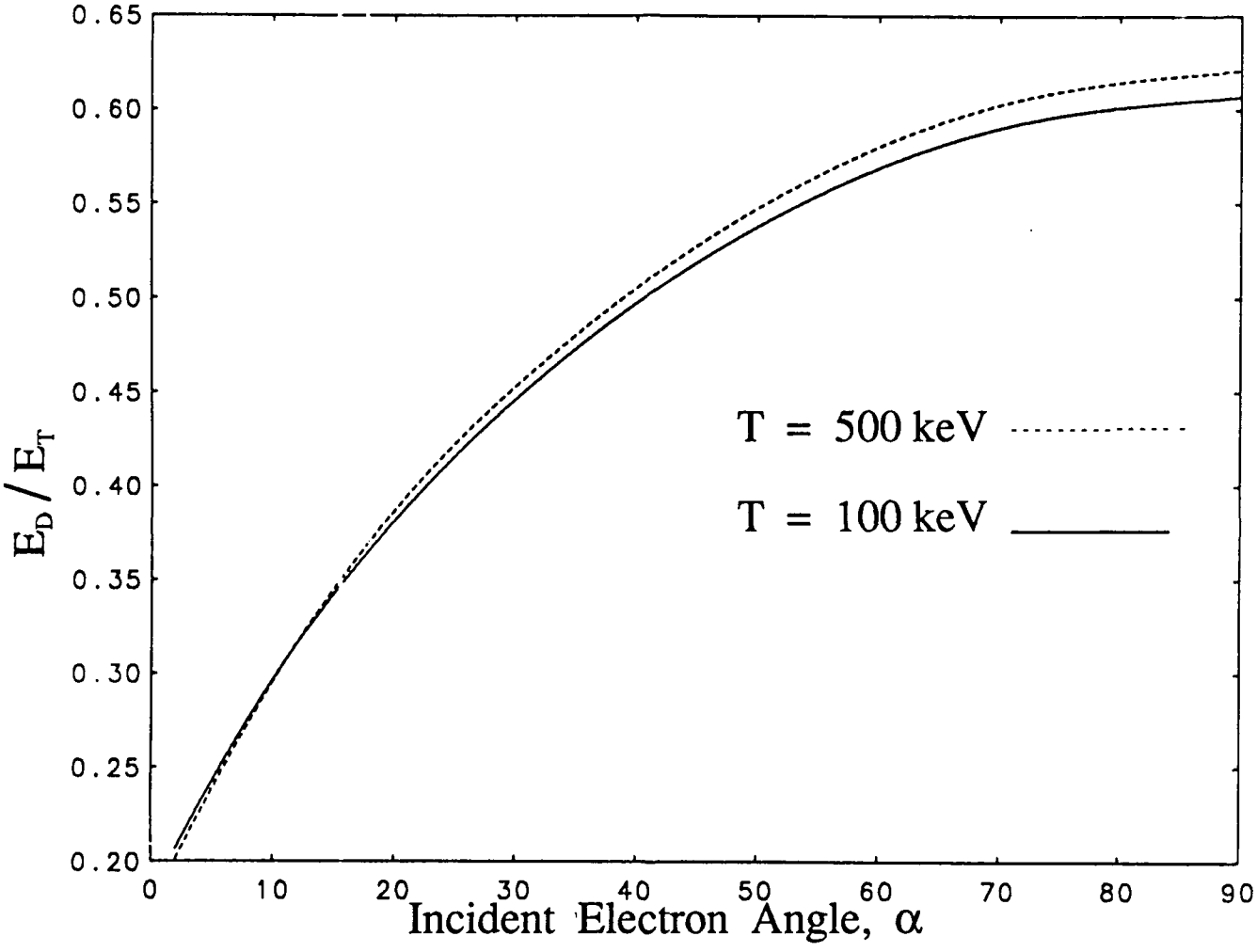

Figure 6. Dependence of the energy ratio of X-ray emission to electron deposition, E_X / E_D, on the incident electron angle, α, for incident electron energies of 50, 100, 150, 200, 300, 400, and 500 keV.

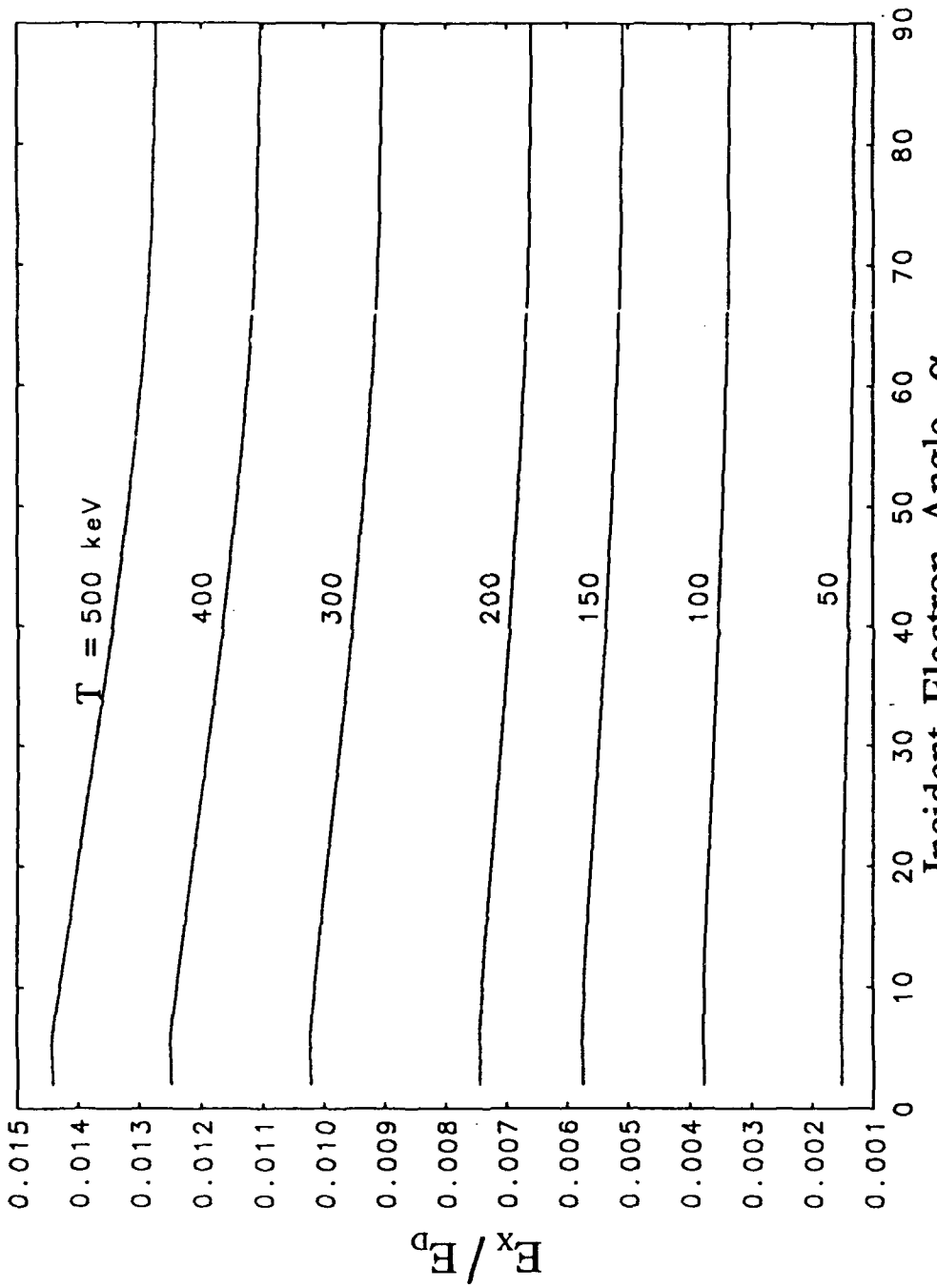

Figure 7. Ratio of X-ray emission energy $E_X(\theta)$, in angular interval from 5 to 10 degrees, to the electron deposition energy, E_D, is a function of the incident electron angle, α, for incident electron energies of 50, 100, 150, 200, 300, 400, and 500 keV.

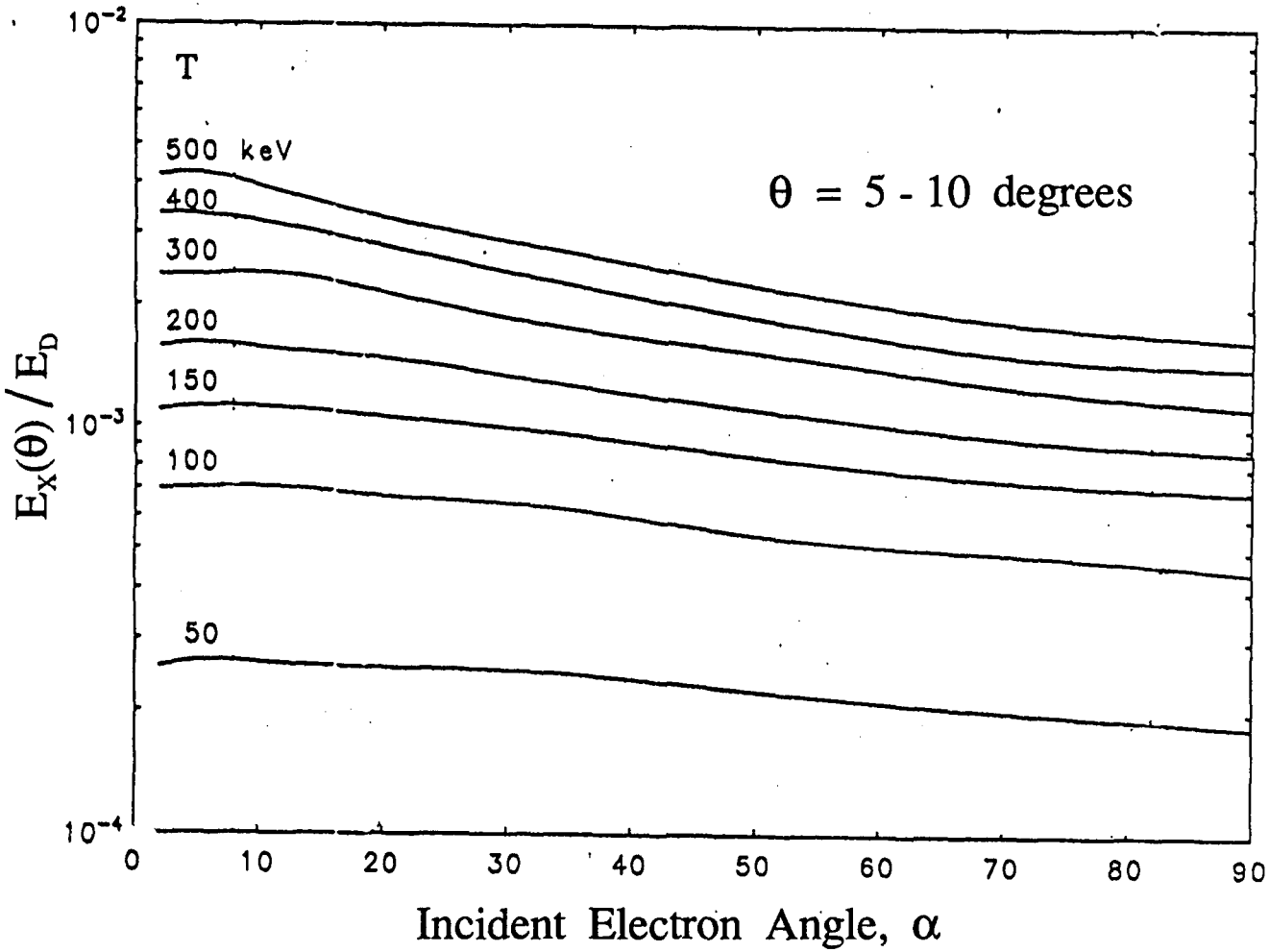

Figure 8. X-ray power enhancement factor for the Enhanced Power (EP) tube over the Standard (S) tube, as a function of tube kilovoltage.

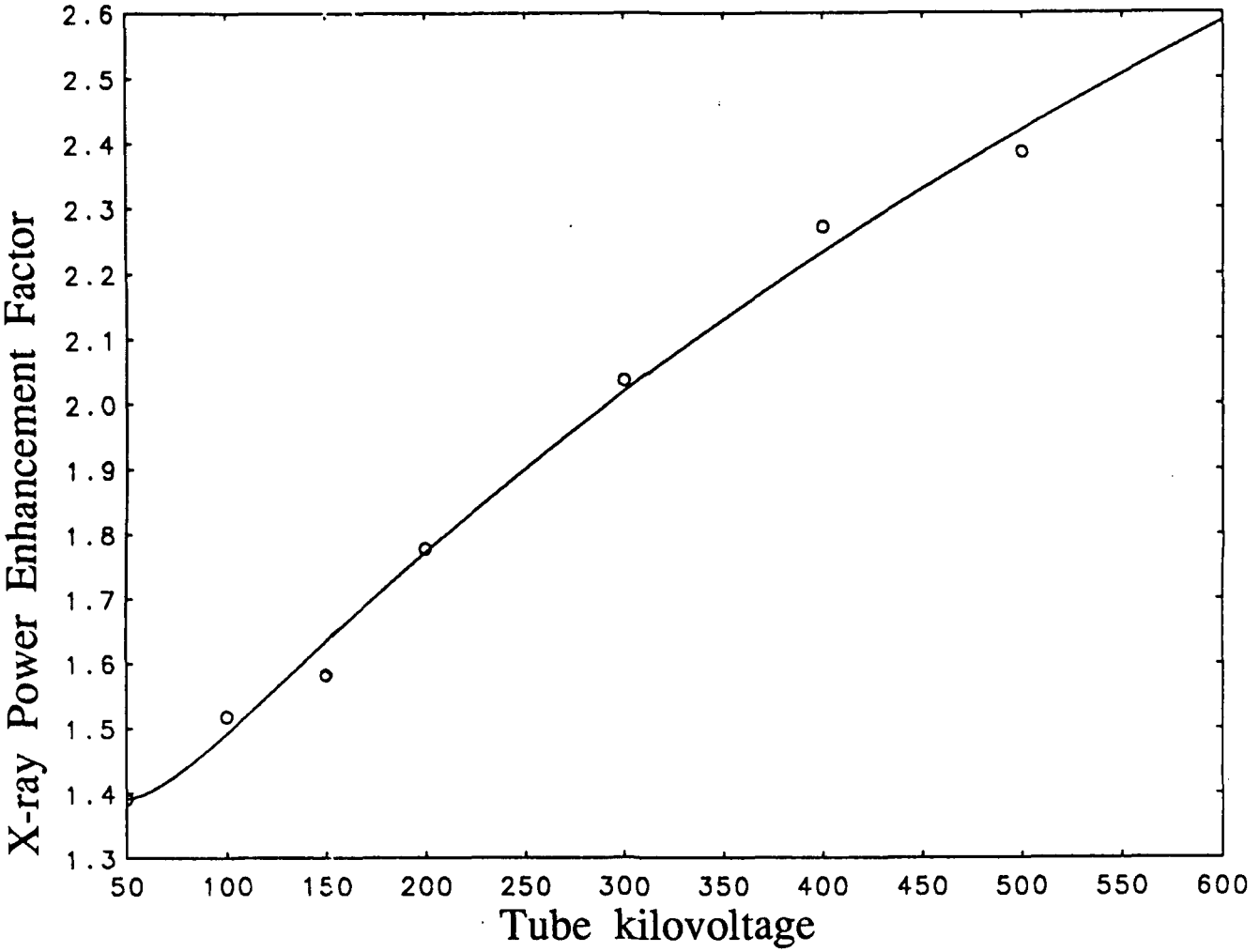

Figure 9. Unfiltered S tube spectrum at 150 KV. N(k,θ) is evaluated for θ averaged over 5 to 10 degrees and α equal to 10 degrees, and gives the photon number per keV per steradian per incident electron.

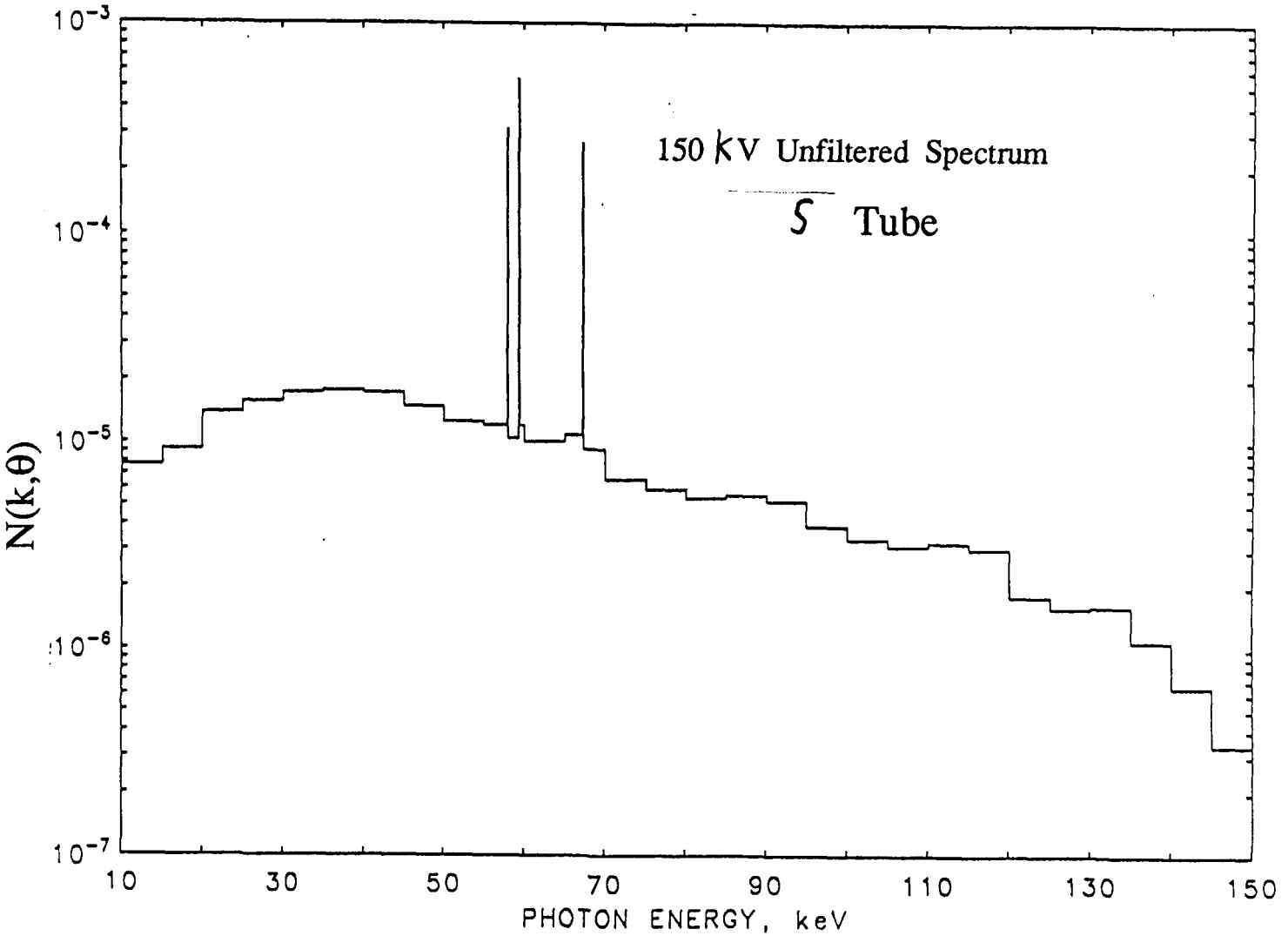

Figure 10. Unfiltered EP tube spectrum at 150 V. N(k,θ) is evaluated for θ averaged over 5 to 10 degrees and α equal to 10 degrees and gives the photon number per keV per steradian per incident electron.

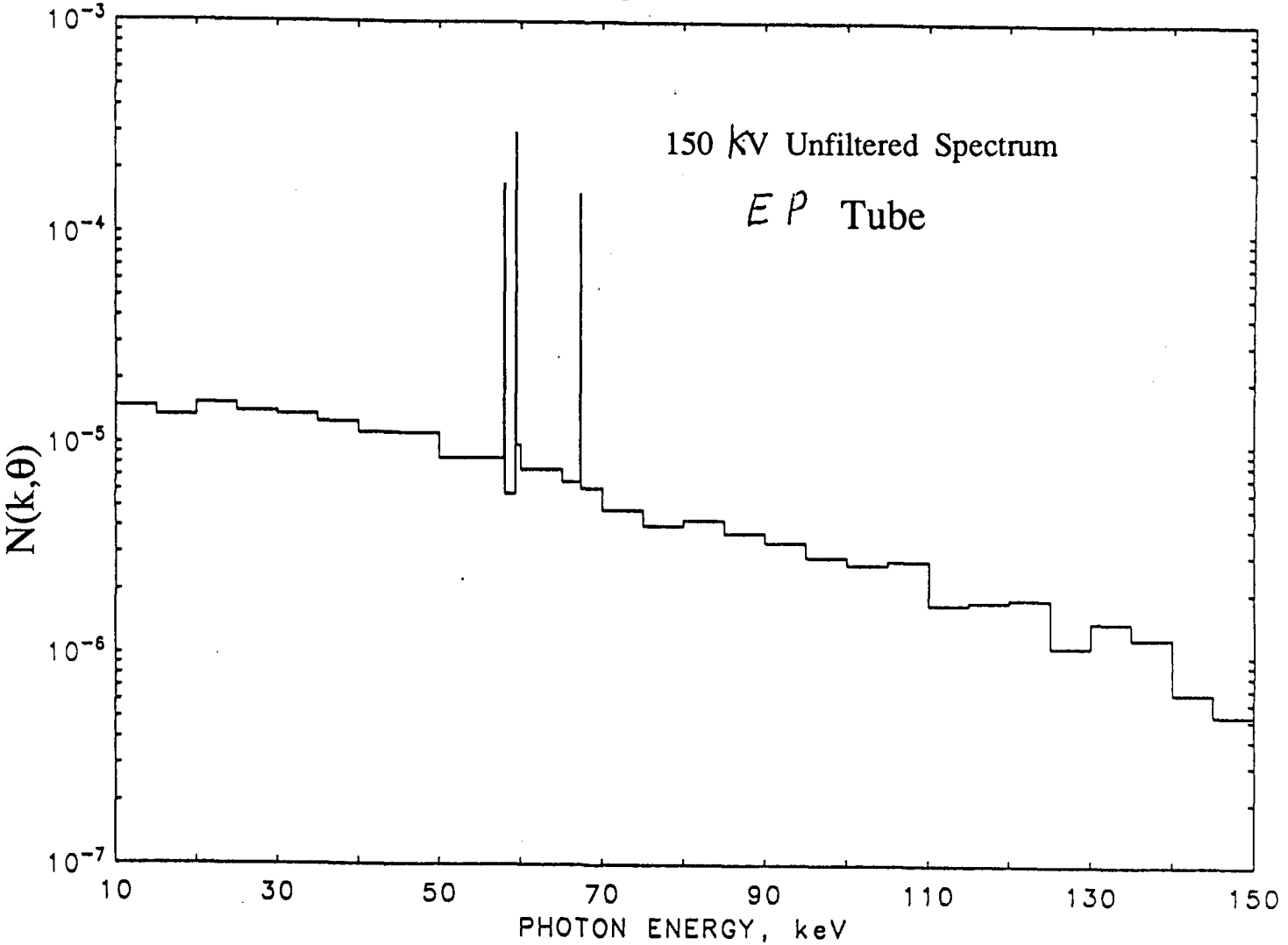

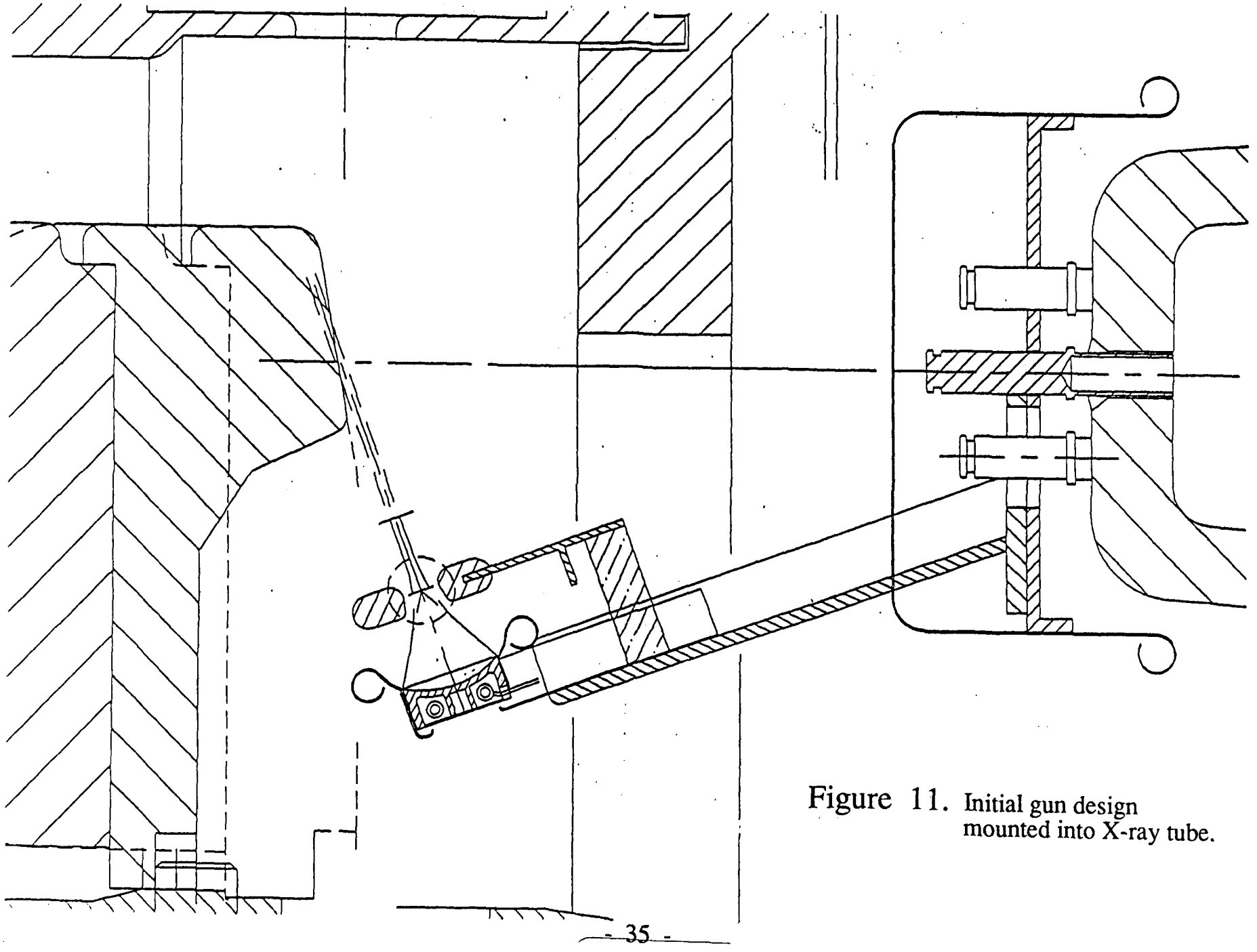

Figure 11. Initial gun design mounted into X-ray tube.

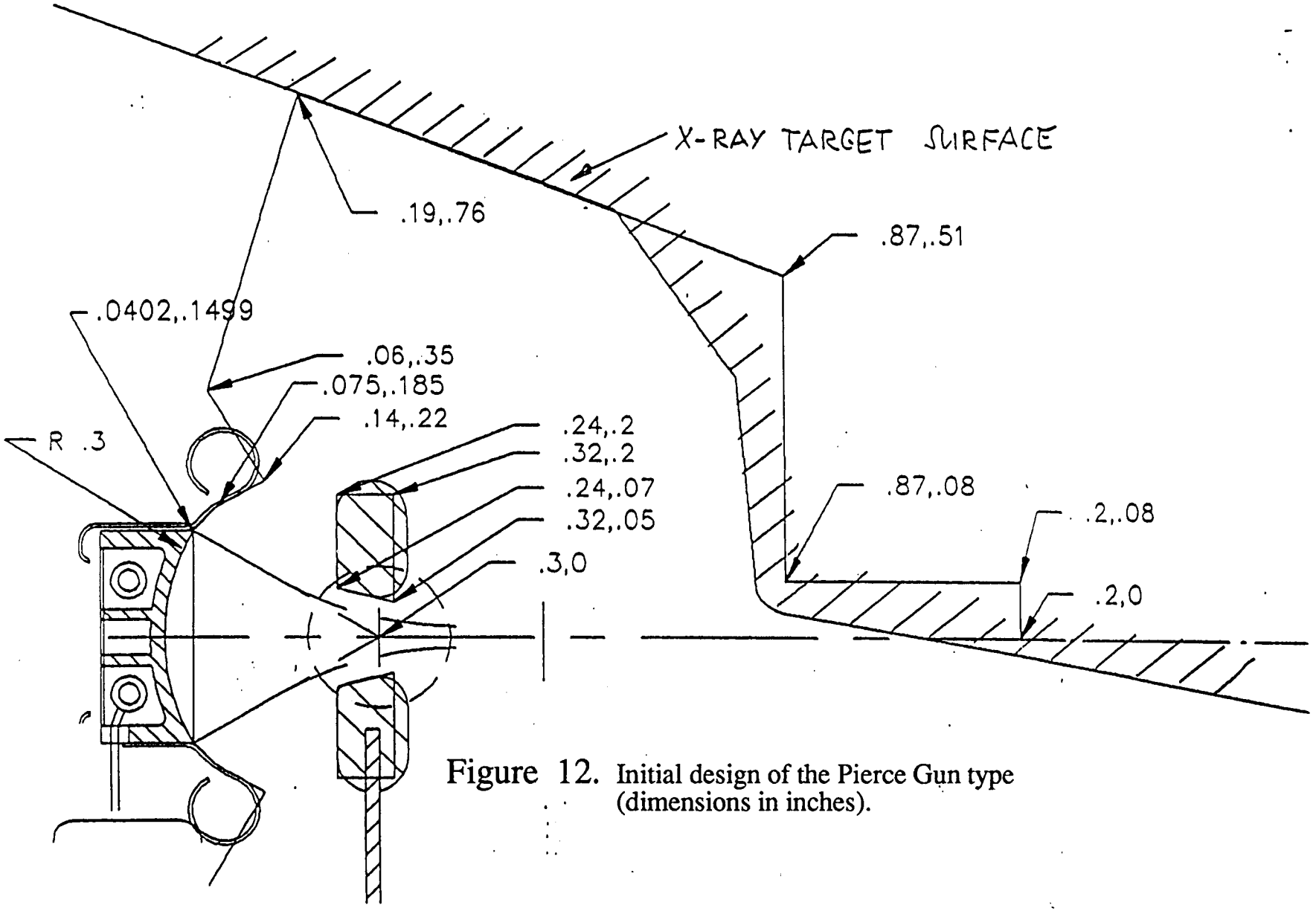

Figure 12. Initial design of the Pierce Gun type (dimensions in inches).

Figure 13. Final electron gun design

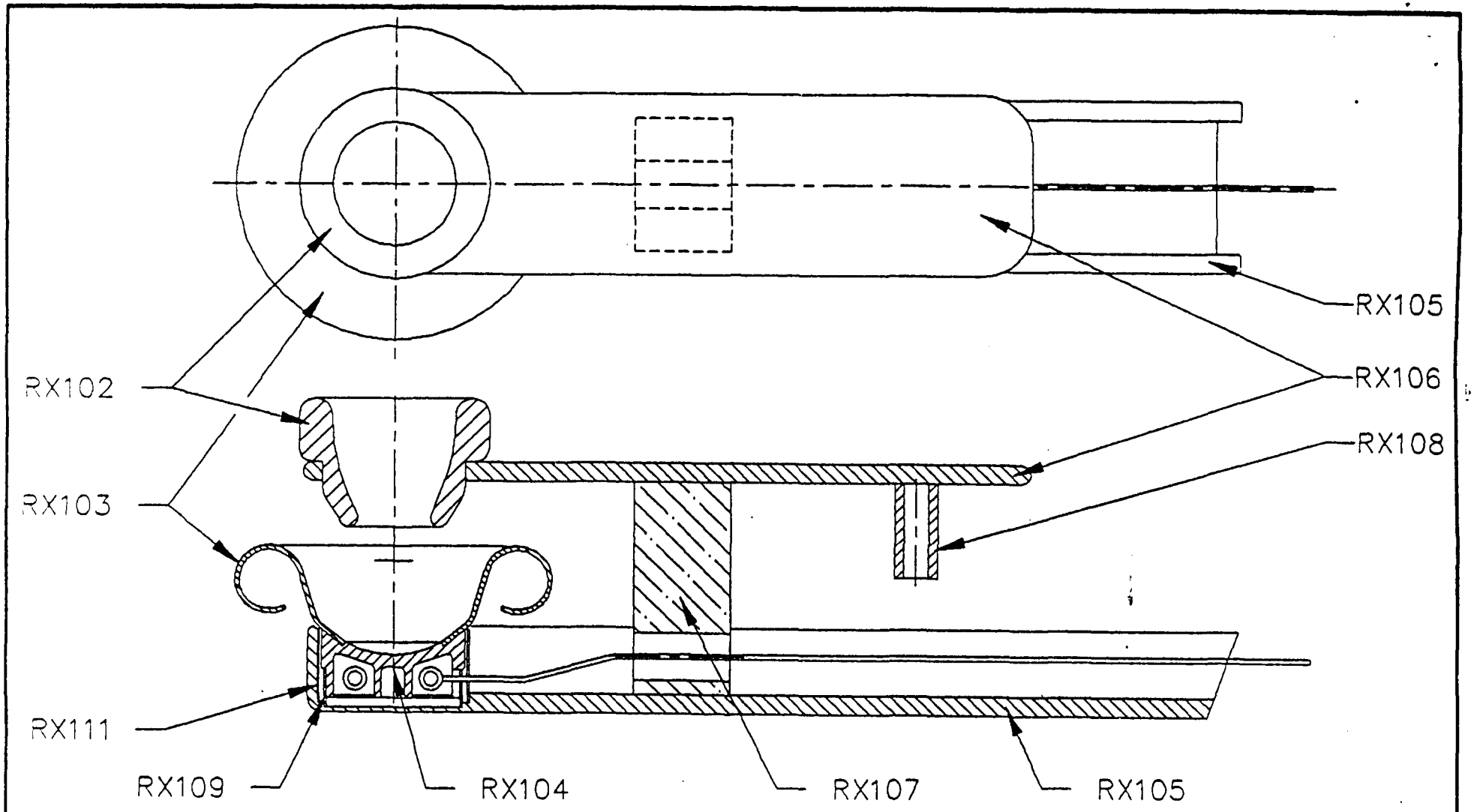

NEXT ASS'Y	THIS DOCUMENT IS THE PROPERTY OF RAYT ANY USE WITHOUT PERMISSION BY RAYT IS PROHIBITED		DATE	REV	INIT'L
			2-4-90	0	
	TOLERANCES UNLESS NOTED .X ±.030 .XX ±.010 .XXX ±.003	MAT'L: RAW DIM:		A	
				B	
				C	
				D	
				E	
L= / H=				F	
SHEET OF				G	

RAYEX GUN 1.2 ASSEMBLY

SIZE	DWG NO.	REV.
000	RX110 –	0

Figure 14. Final electron gun design mounted in X-ray tube

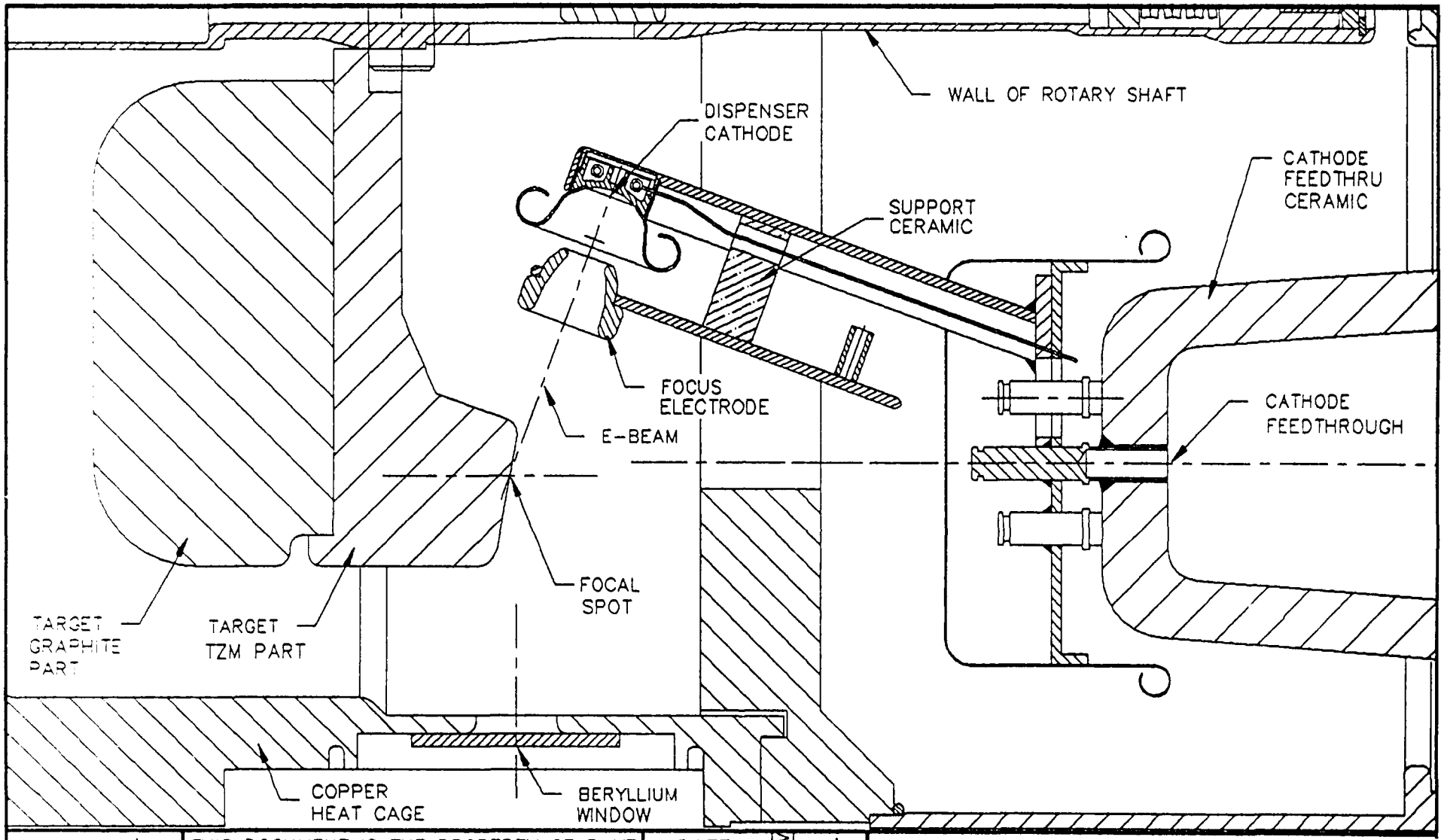

NEXT ASS'Y	THIS DOCUMENT IS THE PROPERTY OF RAYT ANY USE WITHOUT PERMISSION BY RAYT IS PROHIBITED	DATE	REV	INIT'L	
		5-FEB-90	0		
			A		
			B		
			C		
			D		
			E		
			F		
			G		
L= / H=	TOLERANCES UNLESS NOTED .X ±.030 .XX ±.010 .XXX ±.003	MAT'L: RAW DIM:			RAYEX GUN IN X-RAY TUBE
SHEET OF					METAL-CERAMIC X-RAY TUBE MEICOR TYPE
					SIZE 000 DWG NO. RX101 - REV. 0

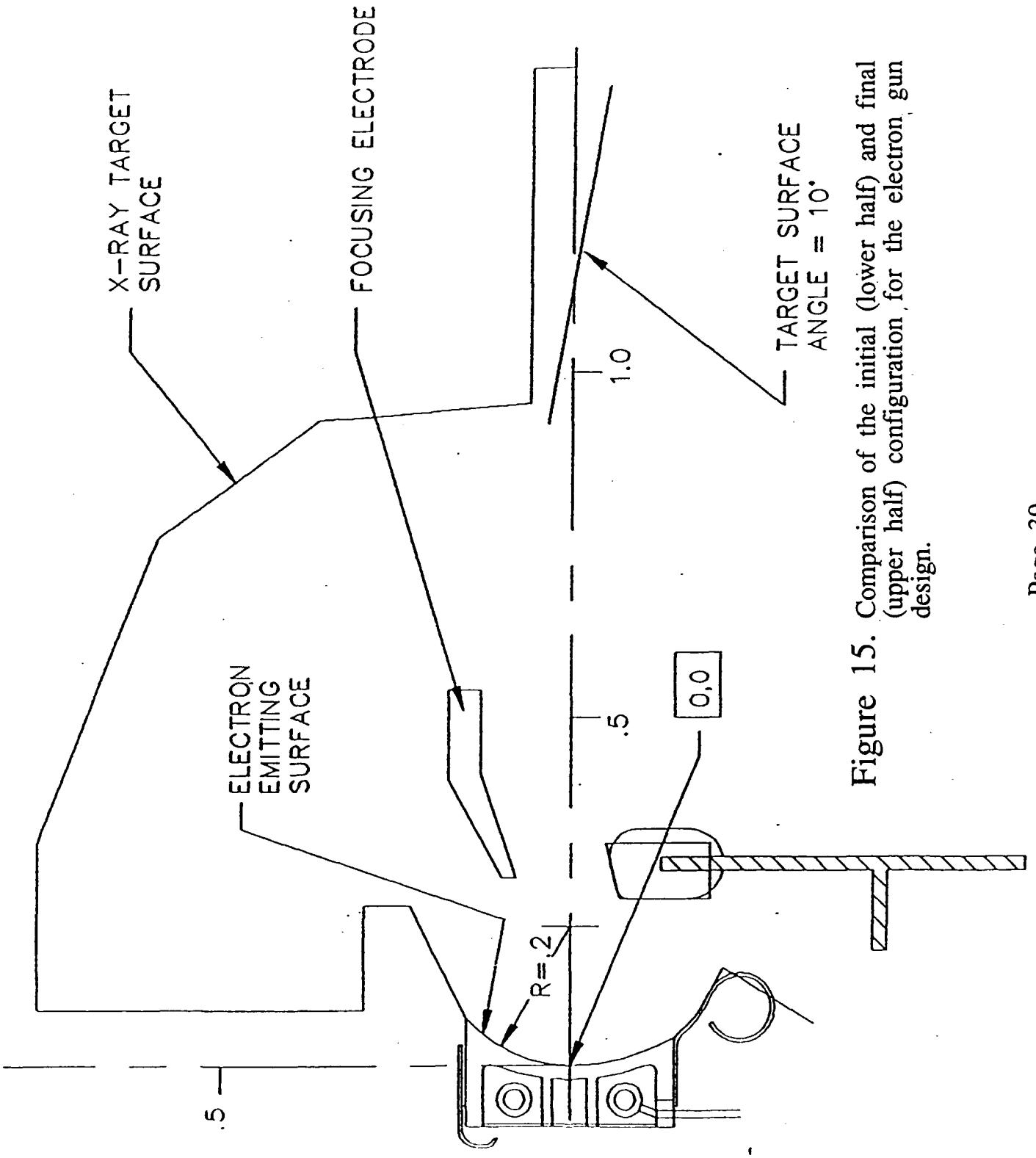

Figure 15. Comparison of the initial (lower half) and final (upper half) configuration for the electron gun design.

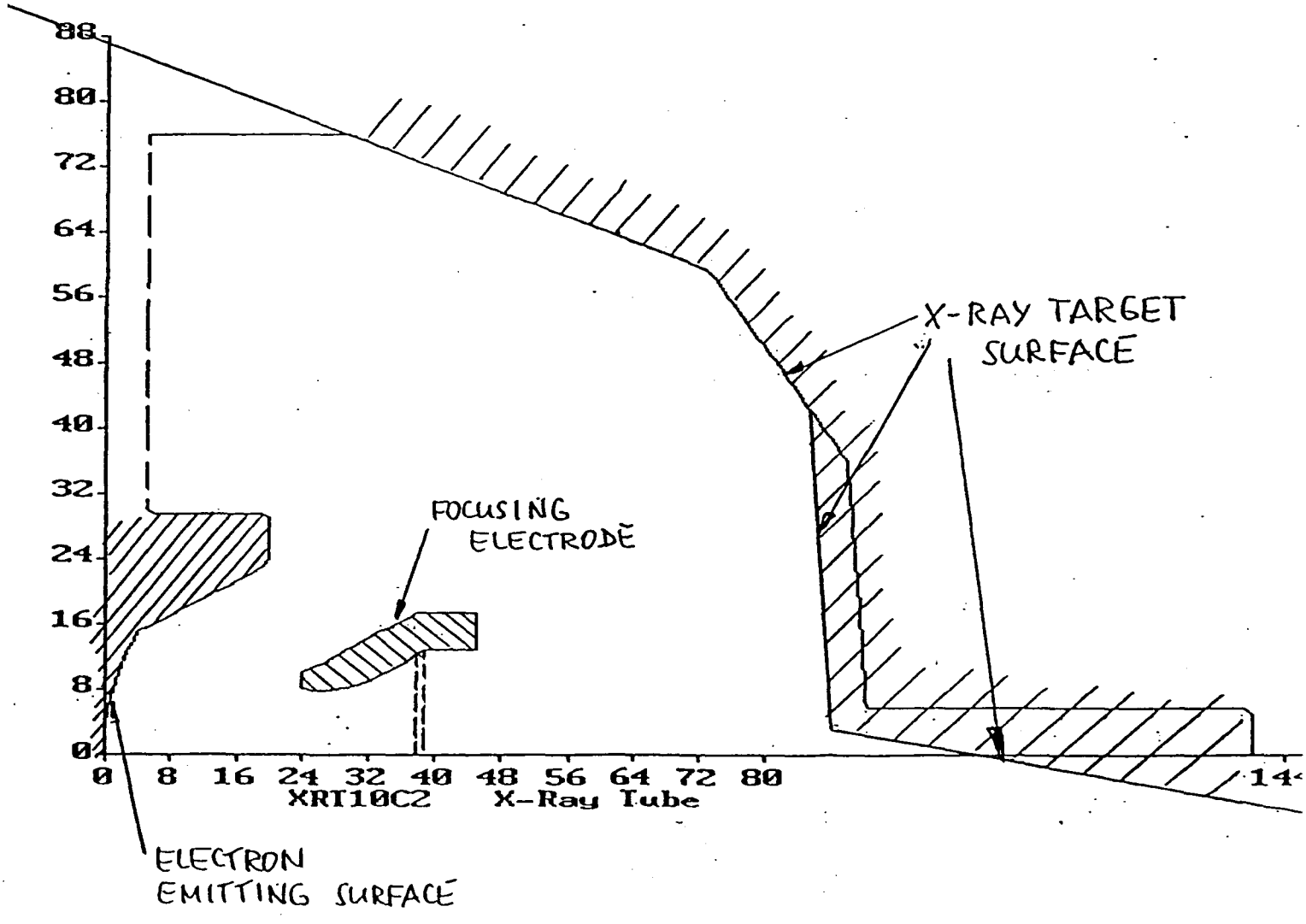

Figure 16. Gun design for computer analysis.

480 mA

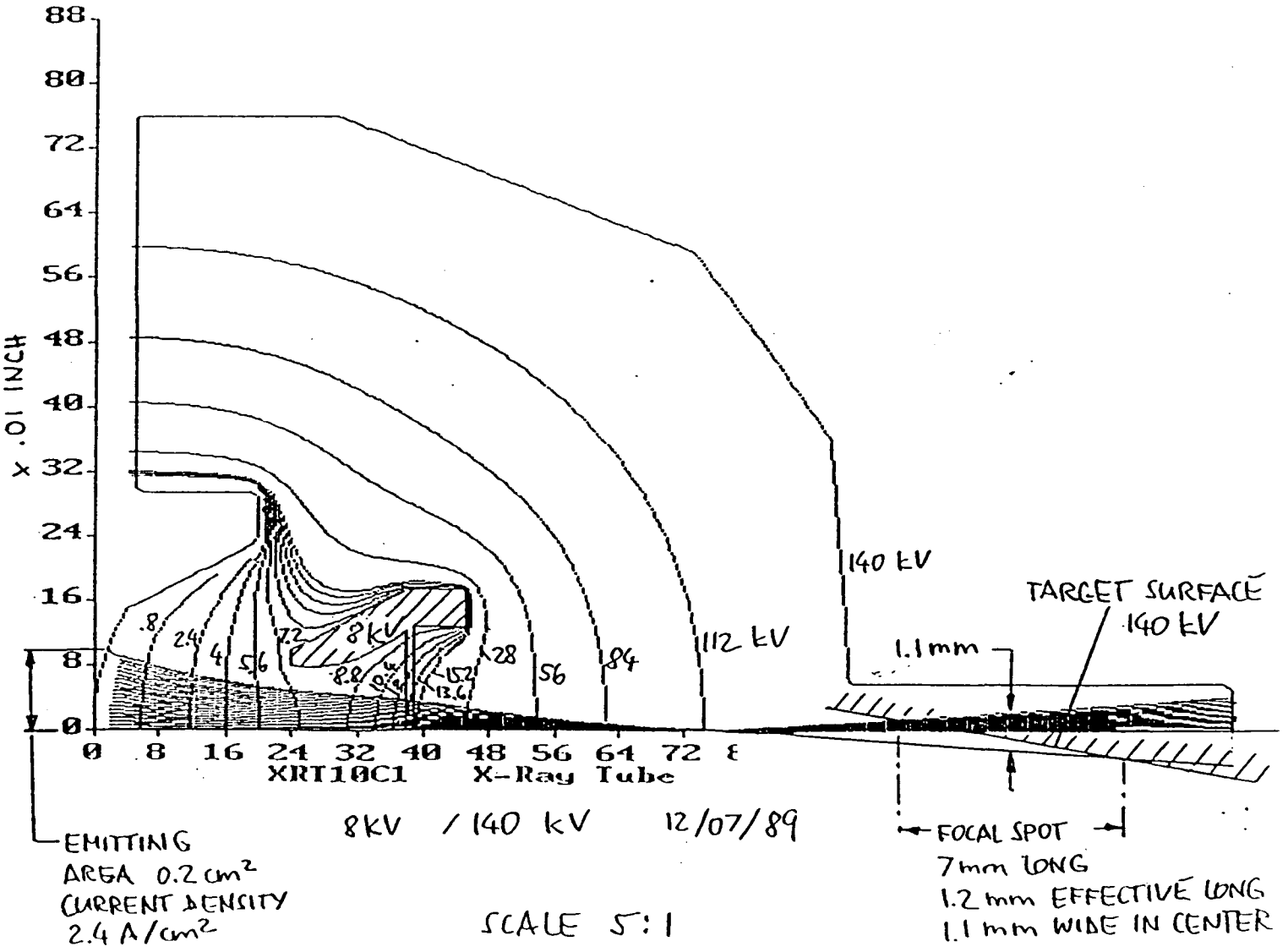

Figure 17. Focal spot dimensions at 140 kV, 480 mA, and 67 kW.

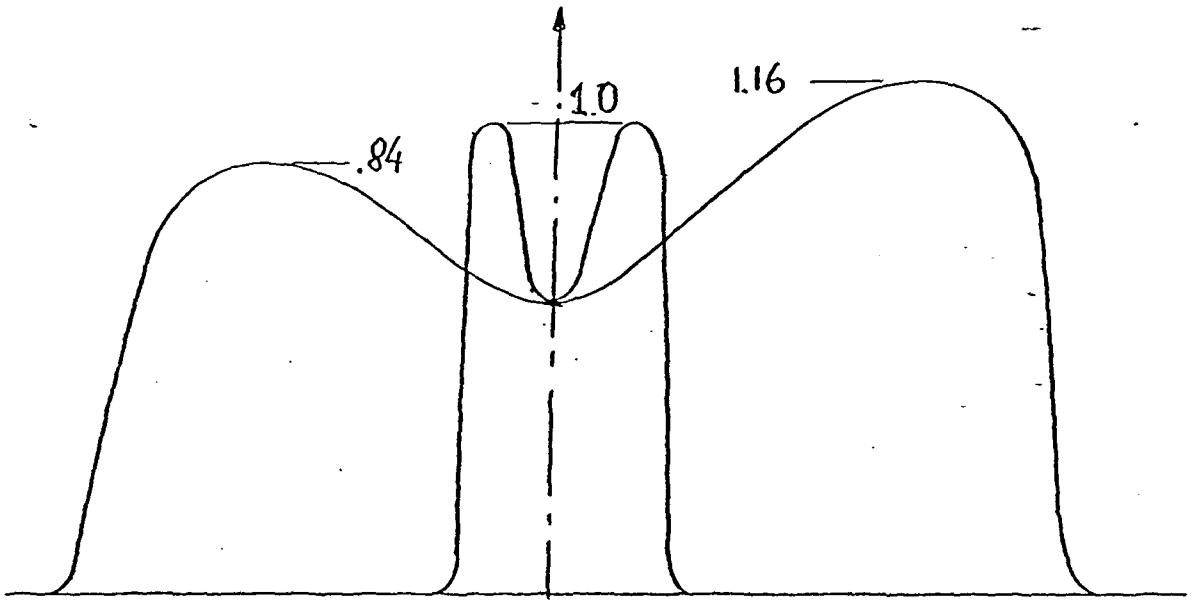

RUN XRT14C2
150 KV. x 170 mA
FOCUS ELECTRODE: 5kV

SPOT SIZE .95 mm × 5.5 mm
PROJECTION FROM 10° TARGET ANGLE:
.95 mm × .95 mm

Figure 18. Electron intensity distribution at the focal spot position.

Figure 19. Computer generated electron beam trajectories at 10 kV / 150 kV.

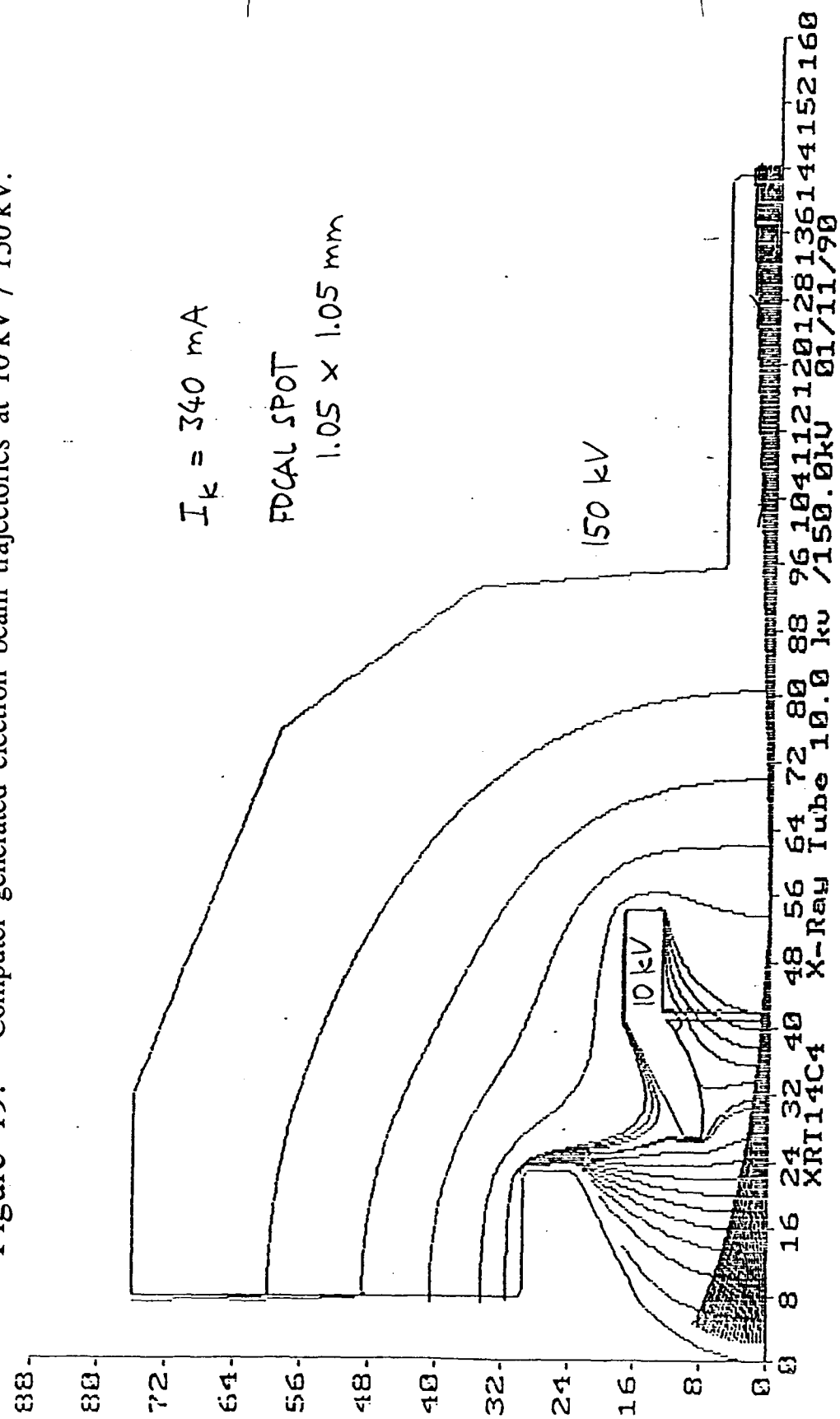

Figure 20. Focus electrode of electron gun for EP tube.

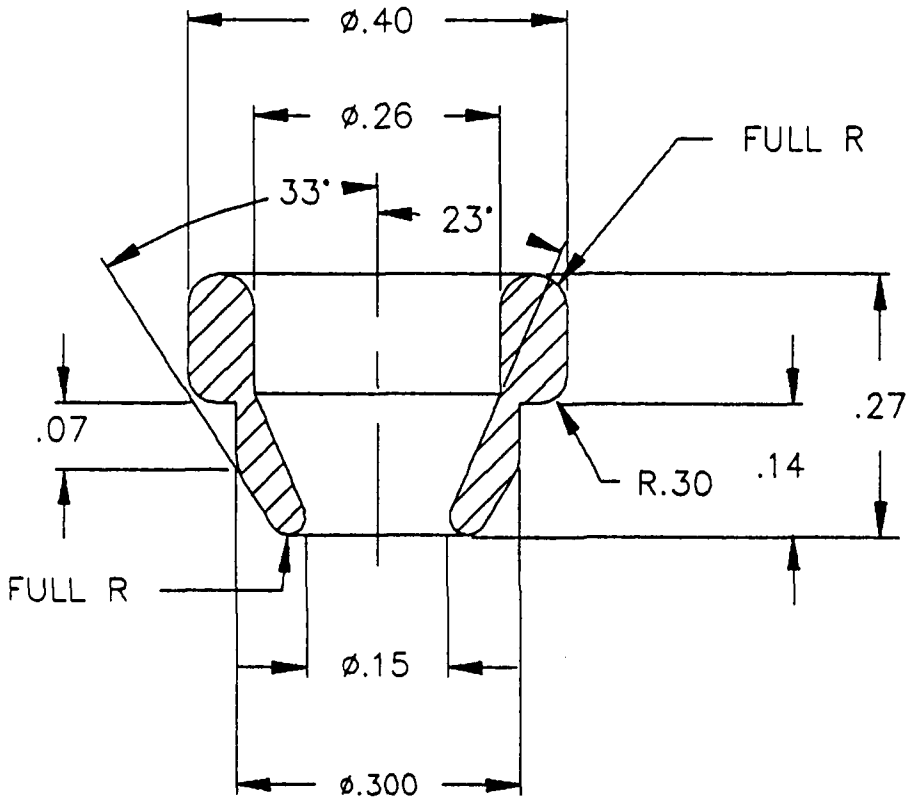

DIMENSIONS IN INCHES

NEXT ASS'Y	THIS DOCUMENT IS THE PROPERTY OF RAYT ANY USE WITHOUT PERMISSION BY RAYT IS PROHIBITED		DATE	REV	INIT'L	
			4-FEB-90	0		
	TOLERANCES	MAT'L: MOLY		A		
	UNLESS NOTED			B		
	.X ±.030			C		
	.XX ±.010	RAW DIM: ø.5 X .3		D		
L= / H= .2	.XXX ±.003			E		
SHEET OF				F		
				G		

FOCUS ELECTRODE
RAYEX GUN

SIZE	DWG NO.	REV.
000	RX102 -	0

Figure 21. Voltage shield of electron gun for EP tube.

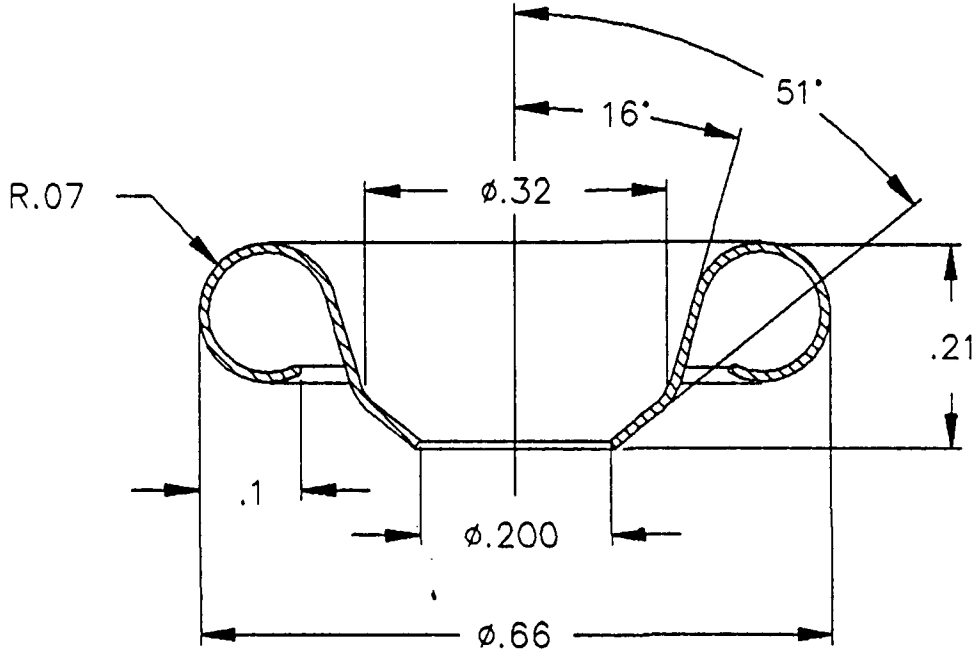

DIMENSIONS IN INCHES

NEXT ASS'Y	THIS DOCUMENT IS THE PROPERTY OF RAYT ANY USE WITHOUT PERMISSION BY RAYT IS PROHIBITED		DATE	REV	INIT'L
			4-FEB-90	0	
				A	
				B	
				C	
	TOLERANCES UNLESS NOTED .X ±.030 .XX ±.010 .XXX ±.003	MAT'L: NICKEL .010TH RAW DIM:		D	
				E	
L= / H= .09				F	
SHEET OF				G	

VOLTAGE SHIELD
RAYEX GUN

SIZE	DWG NO.	REV.
000	RX103 -	0

Figure 22. Dispenser cathode of electron gun for EP tube.

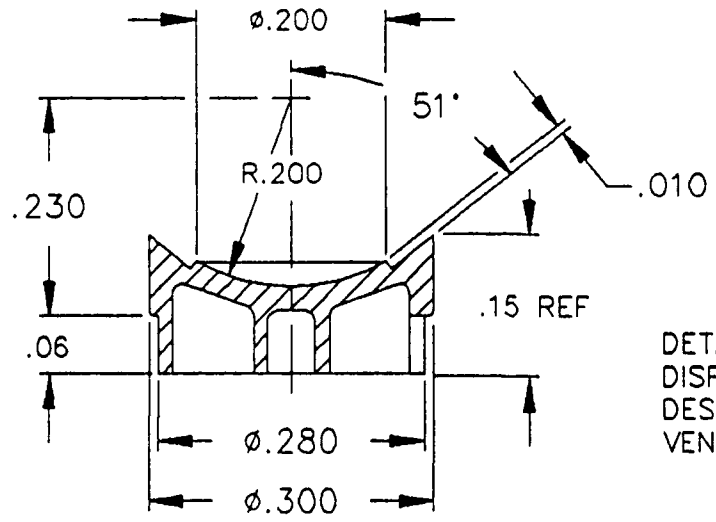

DIMENSIONS IN INCHES

NEXT ASS'Y	THIS DOCUMENT IS THE PROPERTY OF RAYT ANY USE WITHOUT PERMISSION BY RAYT IS PROHIBITED		DATE	REV	INIT'L
			4-FEB-90	0	
				A	
				B	
				C	
	TOLERANCES UNLESS NOTED .X ±.030 .XX ±.010 .XXX ±.003	MAT'L: RAW DIM: ø .300 X .15		D	
				E	
L= / H=.13				F	
SHEET OF				G	

DISPENSER CATHODE
RAYEX GUN

SIZE		DWG NO.		REV.
	000		RX104 -	0

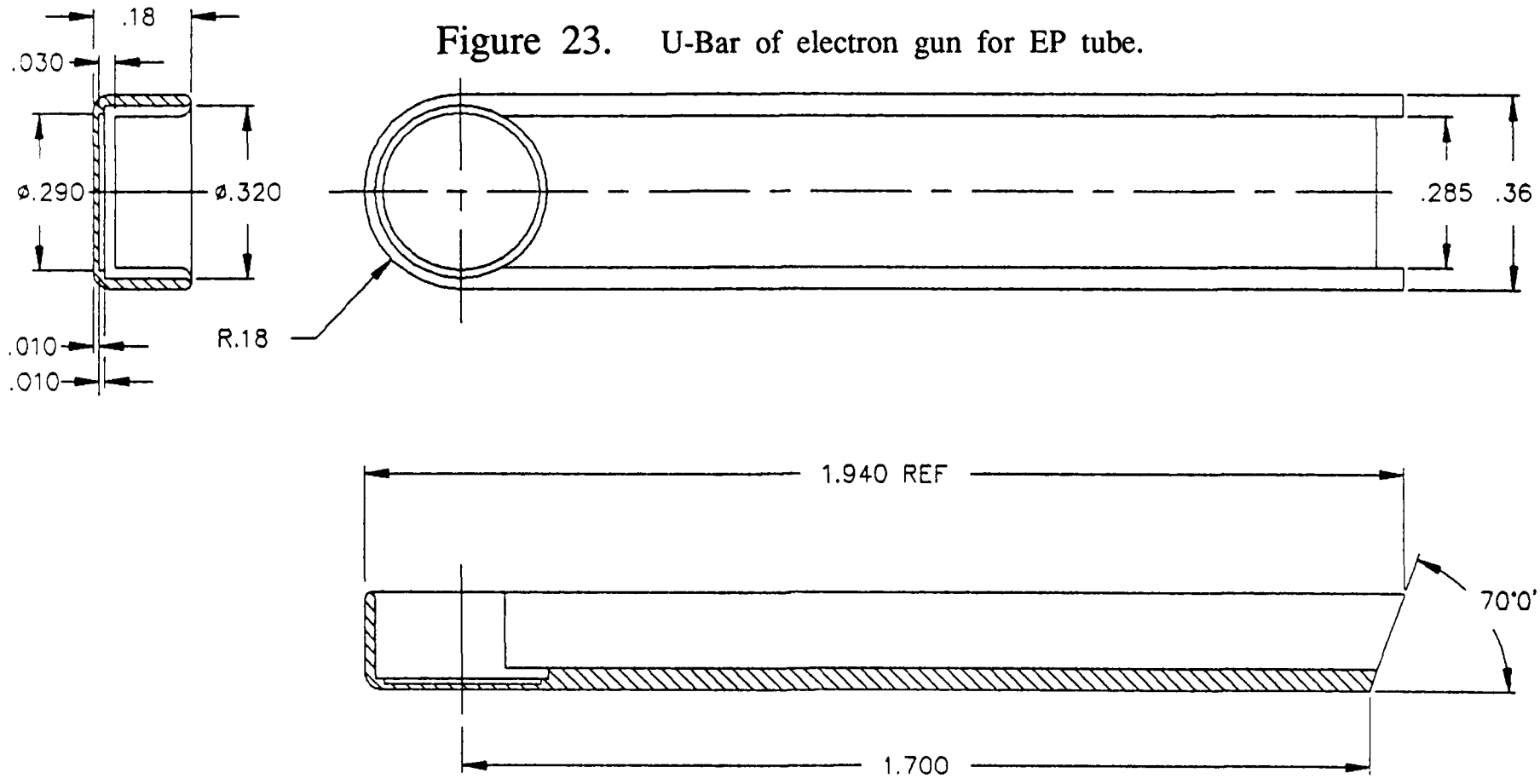

Figure 23. U-Bar of electron gun for EP tube.

DIMENSIONS IN INCHES

NEXT ASS'Y	THIS DOCUMENT IS THE PROPERTY OF RAYT	DATE	REV	INIT'L	
RX110-	ANY USE WITHOUT PERMISSION BY RAYT IS PROHIBITED	4-FEB-90	0		
			A		
	TOLERANCES	MAT'L: KOVAR	B		
	UNLESS NOTED		C		
	.X ±.030		D		
L= / H=.15	.XX ±.010	RAW DIM:	E		
SHEET OF	.XXX ±.003	.2 X .4 X 2.0	F		
			G		

U-BAR
RAYEX GUN

SIZE		DWG NO.		REV.
	000		RX105 -	0

Figure 24. Focus holder of electron gun for EP tube.

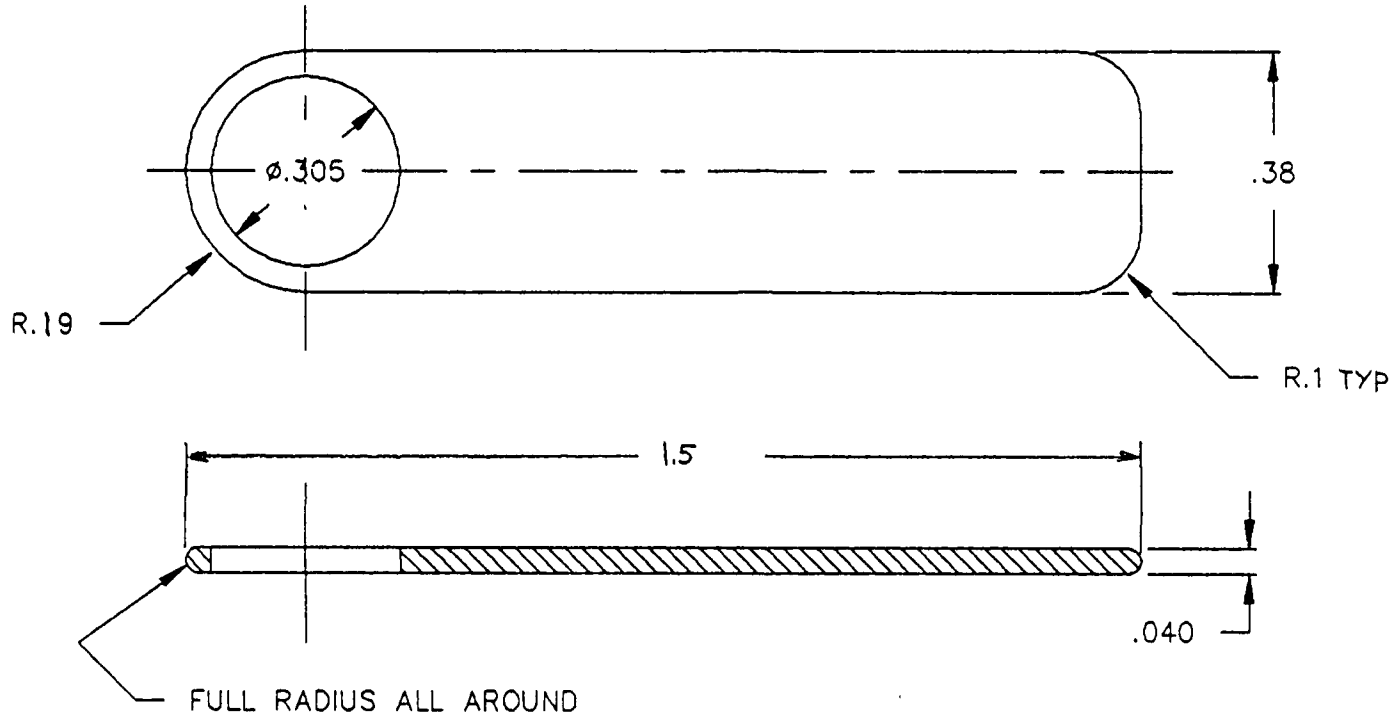

DIMENSIONS IN INCHES

NEXT ASS'Y	THIS DOCUMENT IS THE PROPERTY OF RAYT ANY USE WITHOUT PERMISSION BY RAYT IS PROHIBITED	DATE	REV	INIT'L	
		4-FEB-90	O		
			A		
			B		
			C		
			D		
			E		
			F		
			G		
L= / H=.15	TOLERANCES UNLESS NOTED .X ±.030 .XX ±.010 .XXX ±.003	MAT'L: MOLY RAW DIM: .050TH X .4 X 1.6			FOCUS HOLDER RAYEX GUN
SHEET OF					SIZE 000 DWG NO. RX106 - REV. 0

Figure 25. Ceramic support of electron gun for EP tube.

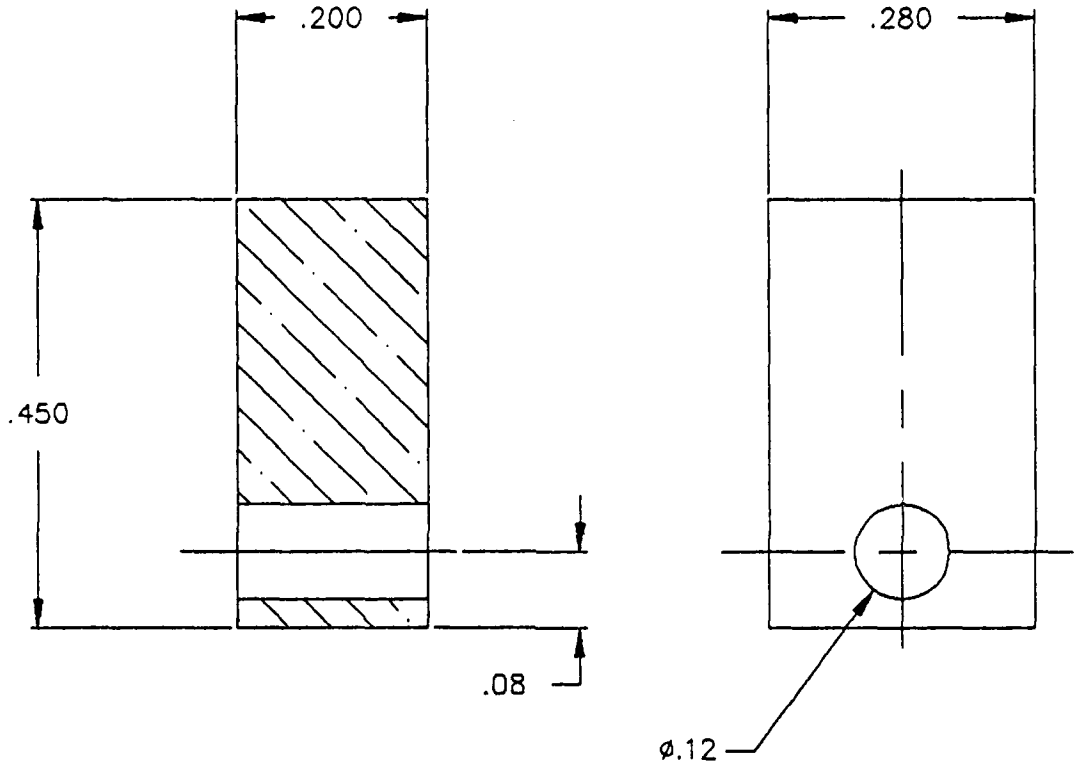

DIMENSIONS IN INCHES

NEXT ASS'Y	THIS DOCUMENT IS THE PROPERTY OF RAYT ANY USE WITHOUT PERMISSION BY RAYT IS PROHIBITED		DATE	REV	INIT'L
			5-FEB-90	O	
				A	
	TOLERANCES UNLESS NOTED .X ±.030 .XX ±.010 .XXX ±.003	MAT'L: ALUMINA95 RAW DIM: .2 x .3 x .48		B	
				C	
				D	
L= / H=.3				E	
SHEET OF				F	
				G	

CERAMIC SUPPORT
RAYEX GUN

SIZE	DWG NO.	REV.
000	RX107 -	D

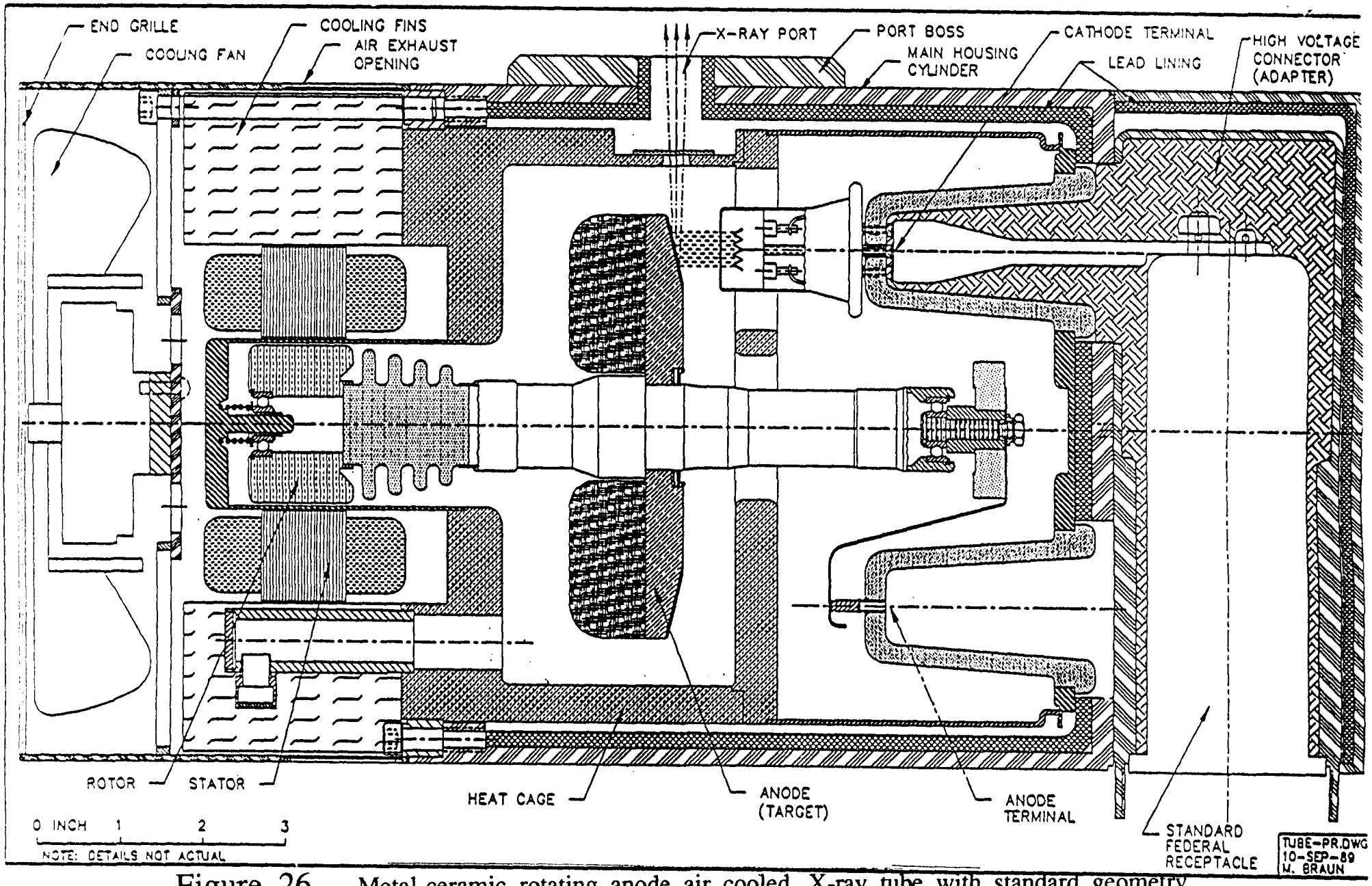

Figure 26. Metal-ceramic rotating anode, air cooled, X-ray tube with standard geometry.

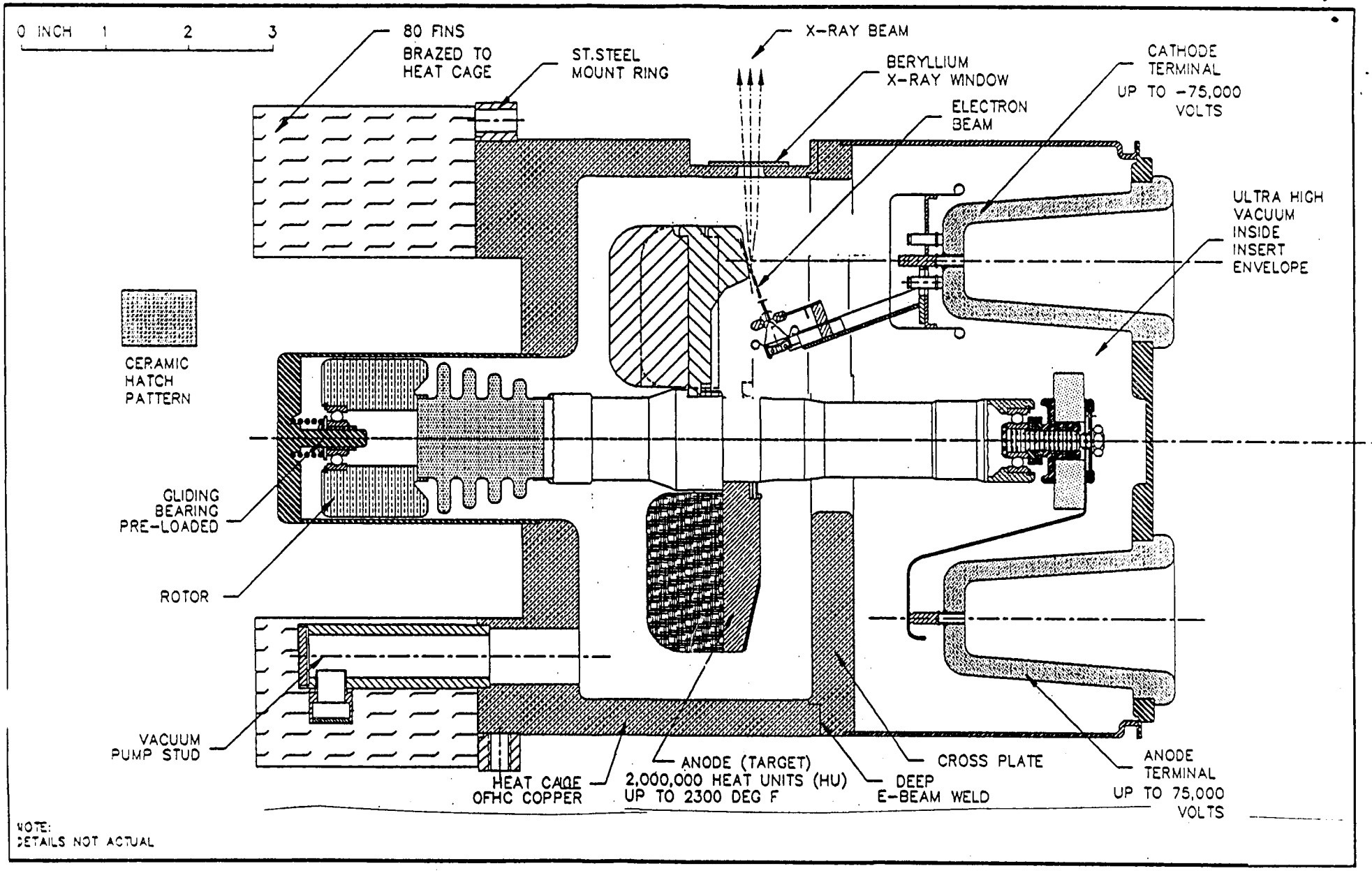

Figure 27. Metal-ceramic rotating anode, air cooled, X-ray tube with EP geometry and initial gun electrode design.